BSc thesis APPLIED MATHEMATICS and APPLIED PHYSICS

"Synchronisation in complex networks"

MASSIMO ACHTERBERG

Delft University of Technology

Supervisors

Dr. J.L.A. Dubbeldam

Dr. M. Blaauboer

Committee members

Dr. N. V. Budko

Prof. dr. Y.M. Blanter

August, 2017

Delft

Contents

Abstract

The main investigation in this thesis is the research on a future quantum internet. The focus is laid on the network structure of this quantum network. The network is first examined by the investigation of the Kuramoto model for classical oscillators. The main property of the network is the ability to synchronise all nodes such that all oscillate with the same frequency. Several parameters of the oscillators are varied to verify why and when synchronisation takes place. After modelling the calculated equations of motion, an interesting conclusion arises. For a symmetric ring network, a stable configuration is not always found but by introducing asymmetric oscillators in the network, the synchronous state can be found. This conclusion leads to the idea that a quantum network requires certain differences in its structure in order to guarantee transmission to take place. Furthermore, the existence of synchronisation heavily depends on the parameters used for the oscillators.

The analysis is then continued in the quantum domain where optomechanical systems are introduced. At first, two systems are connected to each other by a gaseous interaction and an electric interaction via a Duffing circuit. The main investigation is again into the synchronisation, which implies that the operators belonging to both systems behave the same as a function of time. Then several synchronisation measures are introduced to measure the ability of the systems to synchronise. As predicted, both systems synchronise in terms of the operators for each system. Then a quantum network is introduced, where a complex yet efficient network is created. This quantum network is a small world network, where a transmitter node is able to connect to the receiver node by only a few links. Furthermore, multiple transmissions can take place at the same time and links which are not connected do not synchronise with the transmitter node. After modelling this network, the results are in compliance with the theory available.

Challenges for a practical quantum network include the experimental basis of being able to utilise optomechanical systems outside laboratory circumstances. Also, the network should be tested for practical use and expanded in a much larger size both in theoretical analysis as well as in experiments.

1 Introduction

The investigations led by several leading technological companies on the research of the quantum computer are being intensified every year. Last year, Microsoft announced a cooperation between Delft, University of Technology and their own research lab, which will be opened any time soon. From this moment on, all research conducted in this laboratory will be on the technical details of the working of the quantum computer, including the exchange of information.

In the last few years we saw the importance of having a safe and secure information transfer system. Several campaign plans of the American government were found online, but also hackers trying to attack and break down communication systems from companies and buildings via all kinds of ransomware. [3, 4] A future quantum network would be ready to solve all these problems, or at least minimize the consequences of an attack.

Since Microsoft is researching all kinds of different technologies, many different systems and materials are available for the final use of the quantum internet. The actual system should be put into practice and be used by millions of people all over the world. An actual communication system which is ready to be implemented as soon as any technical consequences are gone is not yet available. Aside from the major challenges of making quantum computing available outside laboratory circumstances, a real challenge will be the actual construction of a usable quantum network.

The goal of this thesis is to investigate a formerly proposed method for a future quantum network and to verify whether this system meets the requirements needed for the quantum network to work properly. This is done by first examining general network structures. The first model that will be discussed is the classical Kuramoto model, in which oscillators with a phase and amplitude are connected to other oscillators with a certain strength. The general idea is to conclude whether the network can enhance itself into a synchronous state in which all oscillators have the same frequency. In this way, the oscillators can communicate with each other, since they are in the same state. Important in this section is the heavy dependence on the strength and direction of coupling between the oscillators in the network.

From this solid basis in the classical world, an expansion is made into the quantum regime, where a quantum system arises which needs to be able to fulfil the task of a quantum network. This is done by introducing an optomechanical system with is connected to another optomechanical system via a gaseous interaction and an electrical coupling. In this way, synchronisation between the optomechanical systems can take place. In fact, the operators from the two systems synchronise with each other so that they gradually become equal. It requires some advanced calculations to take quantum effects into account, after which a measurement of quantum synchronisation can be introduced. This principle will then be expanded to a quantum network, in which various nodes and interactions will take place. Then several results will be presented from which conclusions can be drawn to quantify the usefulness of the proposed network structure for a future quantum network.

2 Classical model

In this section, the general idea of the classical model will be explained. This will be supported with visual information as well as some in-depth calculations. These calculations will include calculations for stability as well as numerical verifications of the proposed solutions.

2.1 Introduction to the model

In this chapter, we will be looking into a very special network. A network is a collection of nodes (here: oscillators) and links (interactions). All oscillators are coupled by the so-called Kuramoto model, which was first presented by Yoshiki Kuramoto in 1975. [16] This model is widely used in biological processes and neuroscience. In this model, all oscillators have their own phase θ_i and oscillators can be coupled with each other via a link. Several possible network configurations are possible, in which oscillators are connected to some oscillators and not to others, but here a special case will be examined: the ring network.

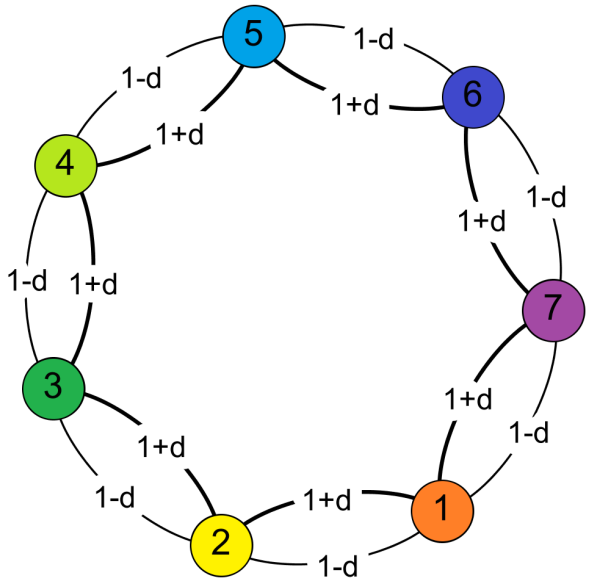

Figure 1: The ring network consists of 7 nodes where each node represents one oscillator. Each node is linked to its two nearest neighbours. All edges are directed **clockwise**, such that node 1 receives input from 2 with strength $1+\delta$ and input from node 7 with strength $1-\delta$. Or to put it differently, with strength $1-\delta$ the information is transferred anti-clockwise in the outer circle and with $1+\delta$ the information goes clockwise in the inner circle. This convention is taken from Pich. [12]

For every network, an adjacency matrix can be constructed. The adjacency matrix **A** contains information on whether a link is connected with a certain weight or not. For example, the adjacency matrix of the ring network above is a 7x7 matrix. When the value in the adjacency matrix in row i is a non-zero value in the j'th column, then oscillator i receives input from oscillator j with weight equal to this value. In this way, the whole matrix is constructed:

$$\mathbf{A} = \begin{pmatrix} 0 & 1+\delta & 0 & 0 & 0 & 0 & 1-\delta \\ 1-\delta & 0 & 1+\delta & 0 & 0 & 0 & 0 \\ 0 & 1-\delta & 0 & 1+\delta & 0 & 0 & 0 \\ 0 & 0 & 1-\delta & 0 & 1+\delta & 0 & 0 \\ 0 & 0 & 0 & 1-\delta & 0 & 1+\delta & 0 \\ 0 & 0 & 0 & 0 & 1-\delta & 0 & 1+\delta \\ 1+\delta & 0 & 0 & 0 & 0 & 1-\delta & 0 \end{pmatrix} \tag{2.1}$$

So node 1 receives input $1+\delta$ from node 2 and $1-\delta$ from node 7. The presented network in Figure 1 consists of 7 oscillators, but the same theory discussed in this paragraph can as well be applied to any number of oscillators. This will be discussed in detail later.

As mentioned before, the oscillators are coupled by the Kuramoto model. The equations of motion for the Kuramoto model are

$$\dot{\theta}_i = \omega + \gamma \sum_{j=1}^{n} A_{ij} \sin(\theta_j - \theta_i) \tag{2.2}$$

where ω is the eigenfrequency of all oscillators and γ the coupling strength between the oscillators. [16] Although this model exhibits several interesting properties, it is rather basic and is not flexible enough. By introducing an amplitude r_i for each oscillator, the equations of motion can be expanded into

$$\dot{\theta}_i = \omega + r_i - 1 - \gamma r_i \sum_{j=1}^{n} \sin(\theta_j - \theta_i) \tag{2.3}$$

$$\dot{r}_i = b_i r_i (1 - r_i) + \varepsilon r_i \sum_{j=1}^{n} A_{ij} \sin(\theta_j - \theta_i) \tag{2.4}$$

where ω is the eigenfrequency of the oscillators (note that this is this same for all oscillators); b_i is the amplitude amplification strength (this will be explained in-depth later); γ and ε represent respectively the coupling strength between the phase and the amplitudes of the oscillators and A_{ij} is the earlier mentioned adjacency matrix indicating the existence of coupling between node i and j. Notice that the phases of all oscillators are connected to all others with coupling strength γ but the amplitudes are only connected by the network structure $\mathbf{A}$. Furthermore, by inserting $r_i = 1$ in Eqs. 2.3 and 2.4 the equations of motion simplify to the original Kuramoto model as in Eq. 2.2.

After introducing the equations of motion for the oscillators in the network, the next section will be explaining a special type of motion and its constraints.

2.2 Synchronization

The oscillators in our model are all oscillating with their own phase and amplitude. However, we are interested in a special oscillation motion in which all oscillators behave independent of time. Mathematically, this implies that $\dot{\theta}_i = 0$ for all i, although the individual phases of the oscillators may be different. We will call this phase-synchronization. This means that all oscillators in the network behave in a steady state solution as shown by Eq. 2.5, which is valid for every oscillator.

$$\dot{\theta}_i = \omega, \dot{r}_i = 0 \tag{2.5}$$

Within this condition given by Eq. 2.5 we can define a new, stronger term which we call synchronization. Synchronization means that all oscillators have the exact same dynamics as a function of time. The exact conditions are given below.

$$\theta_1(t) = \theta_2(t) = ... = \omega t + \theta_0, \tag{2.6}$$

$$r_1 = r_2 = ... = 1 \tag{2.7}$$

Please note that whenever a network has synchronization, it definitely has phase-synchronization. We will see that synchronization won't be achieved instantaneously, but the system will usually converge to the synchronous state instead. The rate of convergence is very important and we will come to that in the next section.

2.2.1 Existence of synchronization

Within this section, we need to make a distinction between the synchronous state and the phase-synchronous state. Showing that the synchronous state exists is straightforward. Simply fill in the conditions given by Eqs. 2.6 and 2.7 into the equations of motion given by Eqs. 2.3 and 2.4 to see that these states are valid solutions.

Phase-synchronization without synchronisation seems to exist systematically, but it actually highly depends on the values of the coupling strength, the network structure and amplitude amplification strength b_i. Analytic calculations to determine whether such states exist are extremely tedious. For a ring network of 2 oscillators, this can be done analytically, see Appendix 2 for more information.

There are enough numerical ways to calculate the existence of phase-synchronous states. Unfortunately this does not yield a nice overview of the possibility of the phase-synchronisation dependant on the unknown variables. We will therefore not calculate these states, but rather observe them in the simulations.

The synchronous state is a much stronger and less common state, but its mathematical existence is much easier to verify. We will therefore examine them in detail in the next section.

2.2.2 Stability

In general, the linear stability of a set of differential equations can be examined by the Jacobi matrix. The Jacobi matrix linearises the set of equations around a point. Here we want to examine the synchronous state, so around $\theta_i = \omega t + \theta_0, r_i = 1$. We then find the following Jacobi matrix.

$$\mathbf{J} = \begin{pmatrix} \gamma\mathbf{K} & \mathbf{I} \\ -\varepsilon\mathbf{L} & -\mathbf{D} \end{pmatrix} \tag{2.8}$$

The matrix $\mathbf{K}$ is the Laplacian matrix corresponding to the all-to-all coupling, so by assuming that all oscillators are coupled to each other. This is the case for the phase interaction, recall Eq. 2.3. Please see Appendix 1 for a complete overview of the Laplacian matrix. The matrix $\mathbf{I}$ is the identity matrix, the matrix $\mathbf{L}$ is the Laplacian matrix which corresponds to the coupling matrix $\mathbf{A}$ which was discussed in Section 2.1. The diagonal matrix $\mathbf{D}$ has diagonal components equal to b_i. The parameters γ and ε are the earlier mentioned coupling strength constants.

In order to verify if stability occurs, we need to look for the eigenvalues of the Jacobi matrix. The eigenvalues of the matrix are generally complex, but we are only interested in the real part, as the real part defines the stability. Furthermore it is known that whenever $Re(\lambda_i) \leq 0 \ \forall i$, the solution is stable. [15]

As mentioned before, the synchronous state always is a valid solution for the set of equations. Furthermore, we can check using Eq. 2.8 that the eigenvalue (call this eigenvalue λ_1) belonging to the synchronous state has value zero. Of course the eigenvector is given by the following relation.

$$\mathbf{v}_1 = (1, 1, ..., 1, 0, ..., 0) \tag{2.9}$$

where the ones belong to the first $1 \leq i \leq n$ coordinates, these are the phases θ_i. The coordinates $n + 1 \leq i \leq 2n$, which are all zeros, belong to the amplitude coordinates r_i. Since we require the solution to be absolutely stable for synchronisation to occur, we may define a new parameter

$$\Lambda = \max_{2 \leq j \leq 2n} Re(\lambda_j) \tag{2.10}$$

where Λ is the maximum Lyapunov exponent which is smaller than 0 when the solution is stable and larger than 0 when it's unstable. [11] Moreover, this exponent defines the rate of convergence to the synchronous state. The more negative the exponent is, the faster the solution converges to the synchronous state. The converse is also true: if the exponent is more positive, the system diverges away faster from this state.

The calculation of the Lyapunov exponent can be done by hand, but the calculation is very tedious and the matrix grows rapidly in size (the size of the matrix is $2n$ for n the number of oscillators in the ring). All stability calculations will therefore be calculated numerically by Matlab.

For the ring network discussed (which is spherically symmetric) the outcome of the result will very possibly be stable. Strangely enough, this is not always true.

2.2.3 Conditions for stability

The formula discussed for stability appears really simple, but tends to behave in a chaotic way in practice. For example, for the ring network with 7 oscillators as discussed in the beginning of this chapter, the Lyapunov exponent is much larger than zero. This is in contrast to what we expect, because a nice, symmetric network will probably give a nice, symmetric result. This exotic behaviour was discussed in detail by Nishikawa and Motter. [11]

By returning to the original problem where 7 nodes are connected in a ring, we define $\gamma = 0.1$ (which indicates a rather weak coupling between the phases of the oscillators) and $\varepsilon = 2$ (which is the amplitude coupling strength). The value for ε does not influence the existence of synchronisation, it only influences the amplitude of Λ. This is discussed in Appendix 4. We will vary the value for b, but keep it homogeneous (i.e. the value for b is the same for every oscillator). Effectively, different parameters of the network are tuned but the network will always remain symmetric. This procedure is shown below.

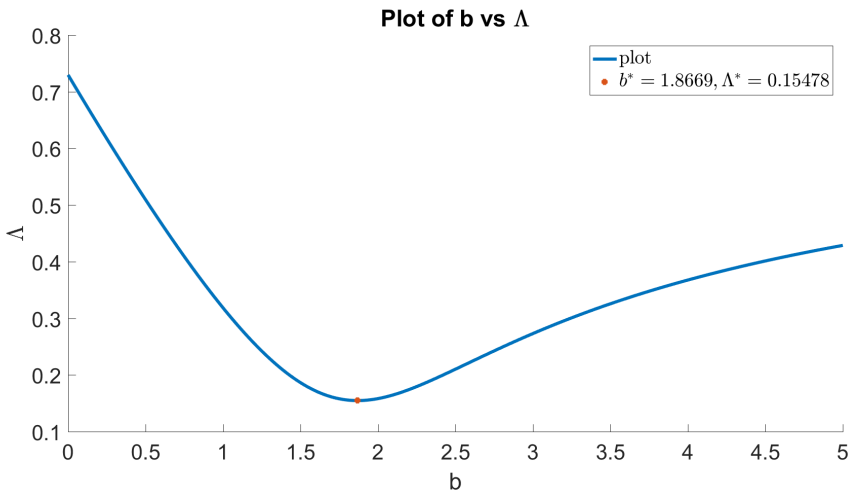

Figure 2: A plot of the Lyapunov exponent Λ for a varying value of b, where b is the same for all oscillators. This implies that the network is symmetric, but it can be seen that for no value of b a stable system will be maintained, since the Lyapunov exponent is larger than zero for all b.

In the plot above, the value for the homogeneous b is varied between 0 and 5 and using the Jacobi matrix, the Lyapunov exponent is calculated. We immediately see that the value of Λ never becomes negative (and thus meaning that the result is stable) and doesn't even get close to it. As an approximation, we see that

the value for b for which the lowest Lyapunov exponent is found, is around $b^* = 1.87$.

So we may conclude that this ring network with these specific parameters cannot yield a stable motion (or, to put it in other words, doesn't synchronize). The interesting thing is, what happens if we choose inhomogeneous values for b? By looking at Figure 2, we may conclude that if a stable configuration exists, it will differ quite much from the original optimal homogeneous b^* since the optimal Lyapunov exponent hasn't reached zero by far. We will therefore try the following procedures:

- Method 1. Fix the same value for b for all oscillators except one. Vary this value for b the same as in the plot above.
- Method 2. Repeat $N = 1000$ times.
    - Generate random b_i from a normal distribution.
    - Keep the b_i if the Lyapunov exponent is lower than the previous best configuration.

This method won't yield optimal values for b_i^* but it does give a good indication of what we can expect. The following plot was constructed for method 1 for a fixed $b = b^* = 1.87$ for the first six nodes and varying the seventh.

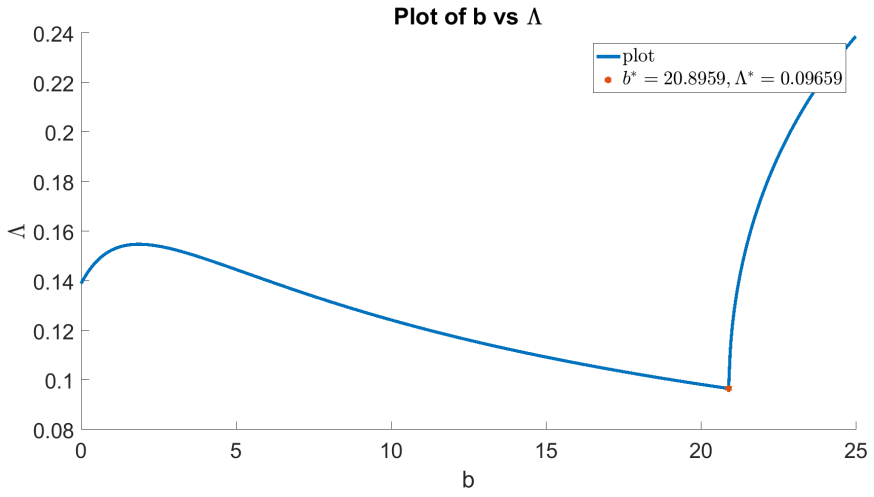

Figure 3: A plot of the Lyapunov exponent for a varying value of b_7, where all other oscillators have the same value $b^* = 1.868$ as found in the previous plot. Since the graph never drops below zero, a stable solution cannot be found using this method.

By looking at Figure 3, a stable solution cannot be found by using Method 1. The conclusion from Figure 2 ("A large deviation from the symmetric solution is required to obtain a synchronous state") can be strengthened by this plot, in the sense that deviating one value for b_i is not enough to achieve this goal. One really requires a real different set of amplification strengths b_i for the different oscillators. The analysis of method 2 will be carried out in the next section.

As a side-note, these findings are not coincidental for this specific ring network. Although it depends on the values of ε and γ, for all ring networks the same conclusion can be found. Appendix 3 contains a list of several ring networks with a different number of oscillators. In all these ring networks, the same principle as discussed above is observed.

2.3 Results

After examining the theory of synchronisation in the last section, we can now head for the results of the evolution of the ring network. In the first subsection we will see the general result of the ring network, after

which we continue to present the corresponding in-depth research and to finish with some remarks about random network structures.

2.3.1 The ring network

First of all, we wish to look into the exact behaviour in time of the ring network with 7 nodes as discussed in the beginning of this chapter. By applying a numerical integration to the equations of motion Eqs. 2.3 and 2.4, the following plot was constructed using Matlab. A link to the Matlab scripts can be found in Appendix 7.

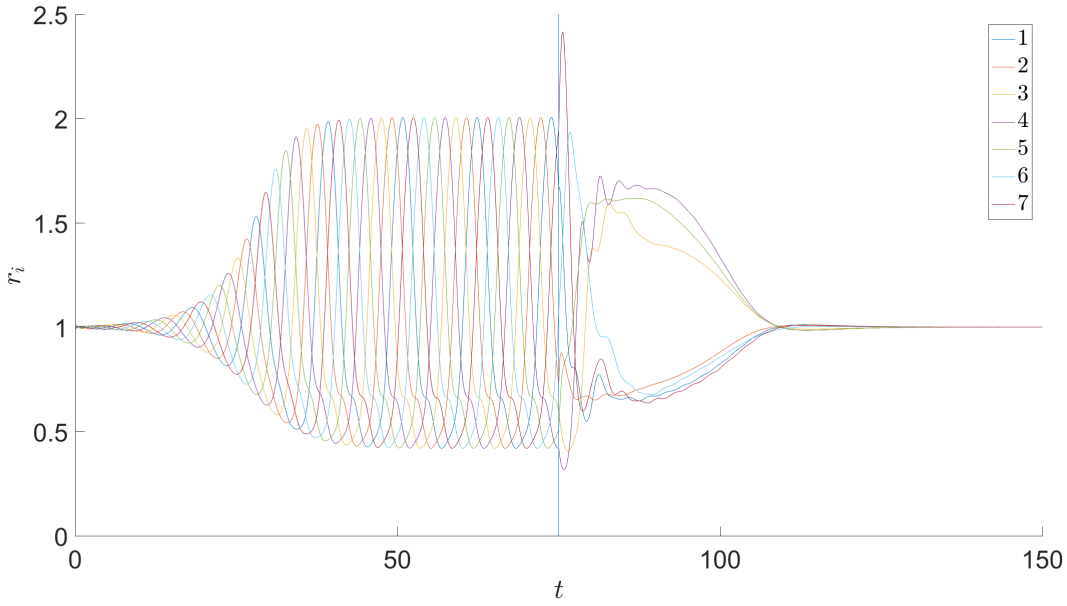

Figure 4: Plot of the amplitudes of all oscillators in a ring network with 7 nodes as a function of time. We have taken the following values: $\varepsilon = 2, \delta = 0.3, \gamma = 0.1$. For $t < 75$, the oscillators in the network are equal with $b_i = b^* = 1.868$. Then, at $t = 75$, all oscillators are chosen with different parameters. See Appendix 3 for the exact values for b_i.

At $t = 0$, we start with a small initial perturbation around the synchronous state $r_i = 1, \theta_i = \omega t + \theta_0$. Here the solution starts oscillating around this point, and after a certain time the solution increases to an amplitude range of about $0.5 - 2$. Here we see the true behaviour of the system, which is called the travelling wave state. Upon the normal perturbation in which all nodes behaves the same, we see a sort of wave going around in the ring and passing all nodes one by one.

After switching to the inhomogeneous oscillators with inhomogeneous b_i at $t = 75$, we first recognize some chaotic behaviour. Rather quickly after that, the solution converges to the stationary point. The rate of convergence depends on the value for Λ. For the homogeneous b, we have $\Lambda = 0.155$ and for the inhomogeneous b_i we have $\Lambda = -0.286$, which is in accordance with Nishikawa and Motter. [11]

The same principle can be observed for the phase. Since the phase increases linearly in time with eigenfrequency ω, we may define the average phase $\langle\theta\rangle$ which is simply the average of all θ_i. By introducing the parameter $\theta_i - \langle\theta\rangle$ we observe the following.

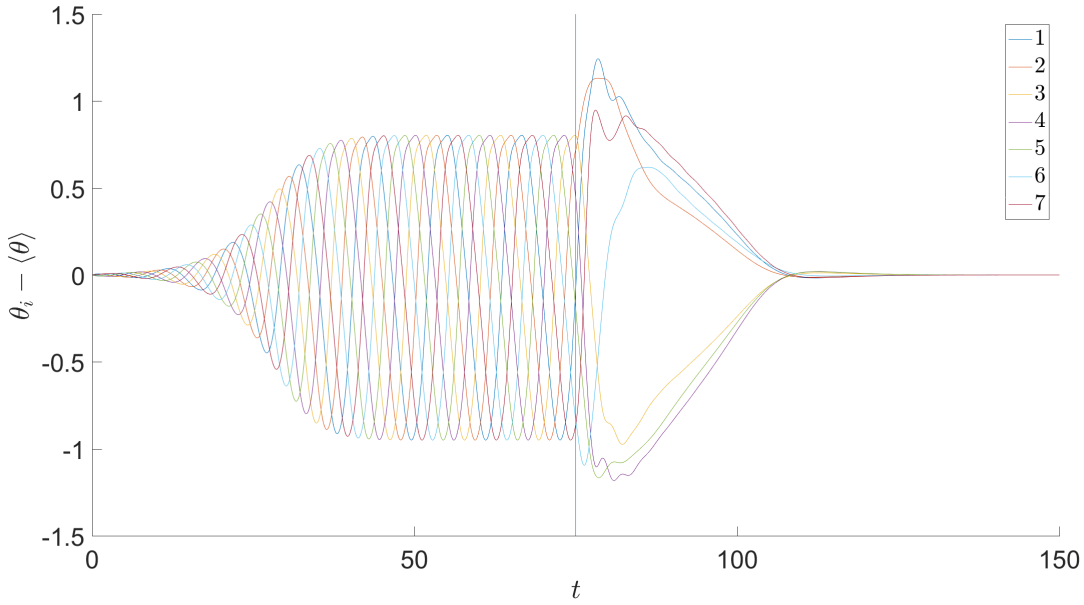

Figure 5: Plot of the phases of all oscillators in a ring network with 7 nodes as a function of time. The parameters are the same as in the previous plot.

This plot shows the evolution of the phase with respect to the average phase $\langle\theta\rangle$ of the system. For $t < 75$, the phase of the individual oscillators follows the average phase, and an extra increase and decrease in frequency is going around in the ring network. This is comparable to the effect visible for the amplitudes of the oscillators. The direction of the ring network which follows from the sign of δ is vital, since the travelling wave state follows this direction.

After switching to inhomogeneous values for b_i at $t = 75$, the solution shows again some chaotic behaviour. Quickly after that, the solution converges to the synchronous state.

The interesting result here is that a symmetric model (represented by $t < 75$ with the homogeneous b) does not tend to stabilize the system; it even starts oscillating in a travelling wave state. On the other hand, for $t > 75$ which corresponds to the inhomogeneous b_i, the solution quickly converges to the symmetric (stable) situation. Although this finding can be verified numerically, it remains counter-intuitive. Symmetric networks and equations should yield a symmetric solution, which is still true since the travelling wave which is going around a symmetric. But making the system less symmetric results in a more symmetric result. This effect can be observed for this specific network and these specific parameters, but the following section will regard other parameters as well.

2.3.2 Further remarks

Mathematically, using the tools discussed in the previous section (the stability analysis) the conclusion from the previous section can be verified. A much more interesting question is: does this result occur for the complete parameter space $(\gamma, \delta, \varepsilon, \mathbf{b})$? It can be shown that the change of a value for ε has a known influence on the stability of the network, even if the network structure is completely random. [11] This is explained in Appendix 4. This reduces the amount of parameters on which the stability depends to $n + 2$.

In order to visualize the stability for any value of the mentioned parameters, one would need a really high dimensional graphing system, as the smallest ring network (with $n = 3$) already requires 5 dimensions. This is impossible in our three dimensional world, such that we require a split up, of which the first is shown in

the following figure.

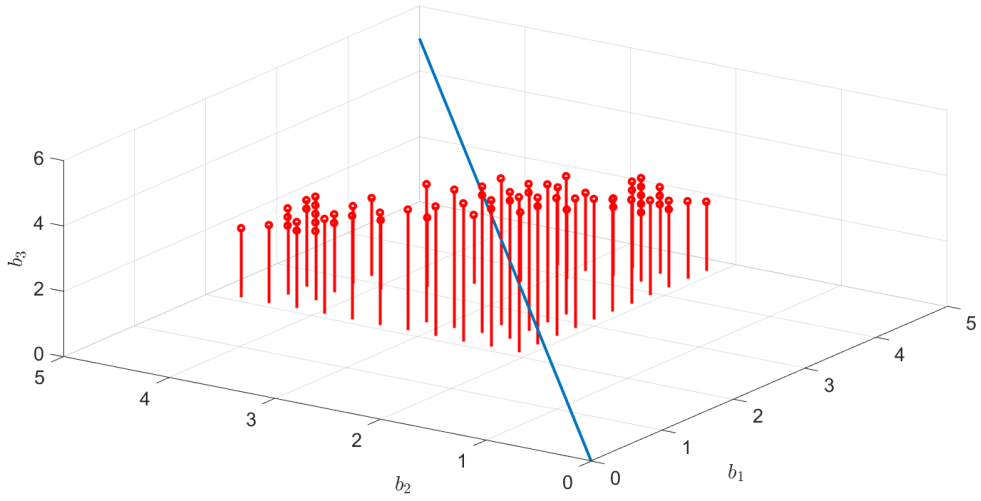

Figure 6: A stability plot of the ring network with 3 nodes with varying b_1, b_2, b_3. The blue line corresponds to the value $b = b_1 = b_2 = b_3$. For each stable combination, a red line with a dot is placed. Only the point indicated by the dot illustrates that this combination of b_i is stable. All points in the plot not indicated with a red dot indicate a positive Lyapunov exponent, hence the system is unstable. Here $\varepsilon = 2, \delta = 0.3, \gamma = 0.65$ and the values for b_i are varied between 0 and 5 in steps of 0.25.

The figure above shows the existence of stable solutions for the ring network consisting of 3 nodes. Since all red dots indicate a stable solution, a large part of the spectrum is not stable because no red dots are present. The figure illustrates the small domain in which the situation presented in this chapter is applicable. Only for a select combination of b_1, b_2, b_3 the system tends to stabilise with a fixed δ and γ. Some further remarks include that the figure is completely symmetric regarding the b values. This is due to the fact that the network is perfectly symmetric, and simply interchanging names between all parameters is possible without any implications on the stability. This argument is clarified by the following figure, which is the same as the previous, except that the view point is taken from above.

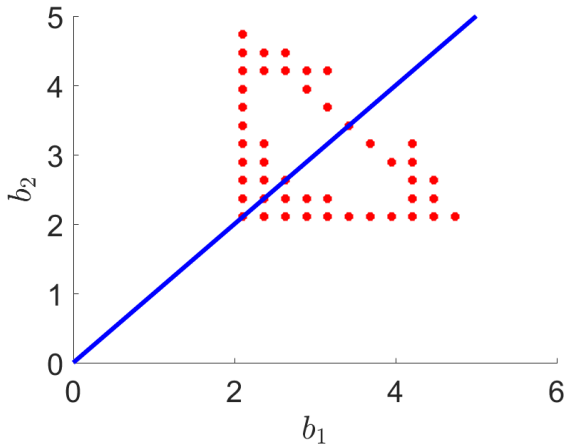

Figure 7: A stability plot of the ring network with 3 nodes with varying b_1, b_2. The blue line corresponds to the value $b = b_1 = b_2$. The plot is the same as Figure 6, but is here projected from above.

The most important conclusion is that the system is not stable for any chosen $b = b_1 = b_2 = b_3$. Admittedly, this is not so clear from Figure 7, but it can be seen from Figure 6. This conclusion is in compliance with the result derived in the previous chapter and also with Motter and Nishikawa. [11]

After varying the amplitude amplification factors b_i of the oscillators, it is time to examine the effect on the stability of the system of the constant γ and δ.

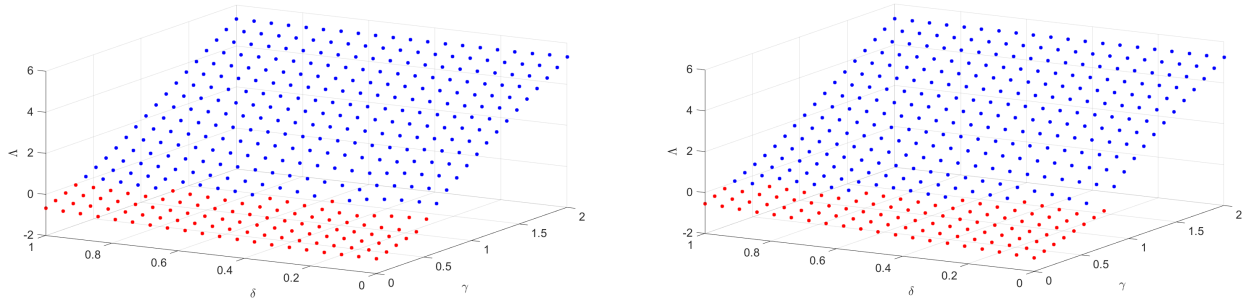

Figure 8: A stability plot of the ring network with 3 nodes with varying γ and δ. The Lyapunov exponent is plotted on the z-axis, where blue points indicate instability and red points a stable system. In both pictures $\varepsilon = 2$ and γ varies between 0 and 2 in steps in 0.1 and δ varies between 0 and 1 in steps of 0.05. In the left picture we took homogeneous values for b and the right picture holds for inhomogeneous values of b_i.

At first glance, both figures seem to resemble quantitatively the same process. However, there are some mentionable differences. For example, the dependence on stability of δ in the homogeneous system (left) is almost not there whereas the right plot shows a more significant drop of Λ as δ decreases. Furthermore, around $\delta = 0.2$ a sudden drop is visible for the homogeneous b. The exact reason for this effect cannot be analysed analytically since the system is far too complex. It does, however, illustrate the chaotic consequences of this ring network in combination with an advanced Kuramoto model.

Generally we may conclude that unstable symmetric systems can be stabilised by choosing asymmetric amplitude amplifications, thus effectively making the network asymmetrical. Apart from this conclusion, we cannot make any further general remarks, since the situation seems to differ per ring network. Also, for asymmetrical, and even random, networks the phenomenon can be observed as well. This concept and a more detailed example of this topic will be discussed in the next chapter.

3 Quantum model

After reviewing the classical approach extensively in the last section, we will now head for the quantum approach. Classically, the goal was to understand and examine all analysis required to understand how synchronisation is used, and now a true application of this principle will be explored. A quantum internet is worked on by several companies and universities, and a quantum internet needs to share (or, to put it in other words, synchronise) its information with other devices connected to the quantum internet.

Where in the classical model all nodes of the system are oscillators, here all nodes consist of much more complex constructions, which will be investigated in detail later on. Just as in the classical scenario, we are interested to find out why and when synchronization takes place between several systems to synchronize quantum information. This principle was first discussed by Mari et al. [10] and a few years later by Li, Li and Song. [9]

In this chapter, at first the interaction between two nodes is discussed. After developing some general tools to investigate the synchronous state in the quantum system, we will continue to link the classical network to a quantum network in which quantum information is transferred. At the end of the section, some general conclusions and observations are drawn for this quantum mechanical information transfer system.

3.1 Introduction to the model

Just as mentioned before, a large difference between the classical and the quantum approach is the difference in the construction of a node. Classically, this was just an oscillator having an amplitude and phase which varies in time. Now, the node consists of a whole system itself, which consists of various different elements. A node is actually a complete optomechanical system. The complete setup for a coupled set of systems is shown in Figure 9.

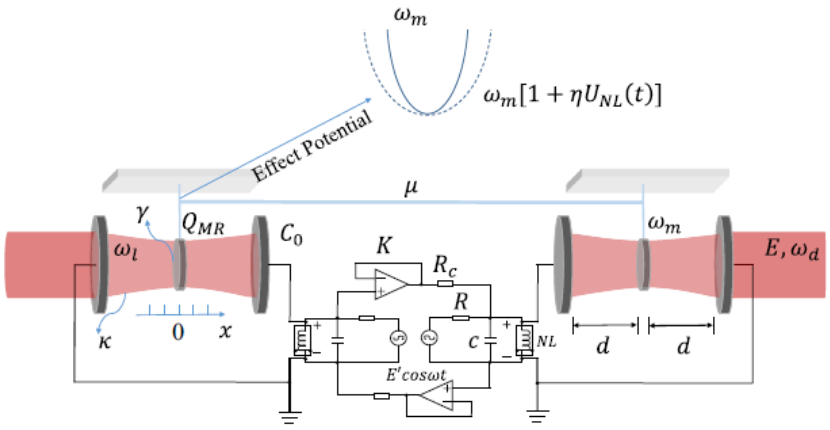

Figure 9: Two coupled nodes in the quantum mechanical system. Each node consists of various electrical, mechanical and optical components. The interaction between the nodes takes place in two forms: the direct electrical interaction with potential difference U_{NL} caused by the circuit and the interaction via the gas inside the cavity via a phonon tunnelling with parameter μ. The electrical circuit is a Duffing circuit and the cavity shown is a Fabry-Pérot cavity. Picture taken from Li, Li and Song. [9]

In order to derive the equations of motion for the optomechanical system, we will need the Hamiltonian to describe its motion. Classically, the Hamiltonian of a system is given as

$$H = T + V \tag{3.1}$$

where T is the system's kinetic energy and V is the potential energy. After switching to a microscopic scale, we need to use the substitutions $x = \hat{q}$ and $\dot{x} = dx/dt = \hat{p}$ which are the operators belonging to the position and momentum of a particle. In this specific model, specific positions or momenta do not exist, hence we define $b(b^\dagger)$ which is the annihilation (creation) operator for the mechanical system. They can best be regarded as ladder operators for counting the number of phonons. Now we may define $b \equiv (\hat{q} - i\hat{p})/\sqrt{2}$. The following relations are known for $\hat{q}$ and $\hat{p}$. [7]

$$[\hat{q}, \hat{q}^\dagger] = [\hat{p}, \hat{p}^\dagger] = 0 \tag{3.2}$$

$$[\hat{q}, \hat{p}^\dagger] = -[\hat{p}, \hat{q}^\dagger] = \hbar \tag{3.3}$$

where $\hbar$ is the reduced Plank constant and it's value is about $10^{26}\, Js$. We can now deduce that

$$[b, b^\dagger] = \hbar \tag{3.4}$$

Although Eq. 3.4 contains an $\hbar$, we will generally switch to natural units, such that $\hbar = 1$ and we leave out $\hbar$ in future equations. Analogue to the mechanical system, we may define the same operators for the optical system. Hence define $a(a^\dagger)$ as the optical annihilation (creation) operators. From this, we define $a \equiv (\hat{x} - i\hat{y})/\sqrt{2}$.

The previous lines denote the basics required to understand the following analysis. It is now time to explore the Hamiltonian. The Hamiltonian will be regarded in terms of the Heisenberg picture and not the Schrödinger picture. In the Schrödinger picture, states evolve in time while the Hamiltonian remains constant. By switching to the Heisenberg picture, the states are time-independent and the Hamiltonian changes in time. This picture allows us to view the change in operators a and b as a function of time which is explained below.

The total general Hamiltonian belonging to optomechanical systems $j = 1, 2$ is given by

$$H = \sum_{j=1,2} (H_{oj} + H_{ej}) + H_{int} \tag{3.5}$$

where H_{oj} is the general Hamiltonian of optomechanical system j, H_{int} is the Hamiltonian corresponding to the gaseous interaction between system 1 and 2 and H_{ej} is the interaction between system j and Duffing circuit j. The general Hamiltonian for the optomechanical system is given by [1]

$$H_{oj} = \omega_{lj} a_j^\dagger a_j + \omega_{mj} b_j^\dagger b_j - g a^\dagger a_j (b_j^\dagger + b_j) + iE(a_j^\dagger e^{-i\omega_{dj} t} - a_j e^{i\omega_{dj} t}) \tag{3.6}$$

where ω_{lj} is the frequency of the cavity mode of system j, ω_{dj} the frequency of the laser driving of system j, ω_{mj} the frequency of the mechanical system j, $a_j(a_j^\dagger)$ the optical annihilation (creation) operator, g is the optomechanical coupling constant and E the laser driving intensity. By applying the rotating wave approximation, in which we switch from a stationary point of view to rotating ourself with frequency ω_{dj} in the optical domain, we find

$$H_{oj} = -\Delta_j a_j^\dagger a_j + \omega_{mj} b_j^\dagger b_j - g a^\dagger a_j (b_j^\dagger + b_j) + iE(a_j^\dagger - a_j) \tag{3.7}$$

where $\Delta_j = \omega_{dj} - \omega_{lj}$. The interaction with the electric network in the system j denoted by H_{ej} is given as

$$H_{ej} = \frac{\omega_{mj}}{4} C_j(t)(b_j^\dagger + b_j)^2 \tag{3.8}$$

which actually is the extra part introduced in this Hamiltonian due to the electrical system. [9] The variable $C_j(t) = \eta\, U_{NL,j}(t)$ depends on the parameters of the electrical components of the circuit η and the voltage $U_{NL,j}$ of the optomechanical system j. This voltage is due to the Duffing circuit belonging to node j. Since Duffing circuits have been analysed extensively due to their non-linear effects, the equation for $U_{NL,j}$ is

known. [9] Actually, this equation is a second-order differential equation, but it can as well be split up in a system of first order equations which is listed below

$$\frac{d}{dt}\phi_j = U_{NL,j} \tag{3.9}$$

$$\frac{d}{dt}U_{NL,j} = -\varepsilon U_{NL,j} - \phi_j - \nu\phi_j^3 + \mathbb{E}\cos(\omega_0 t) + \varepsilon K(U_{NL,3-j} - U_{NL,j}) \tag{3.10}$$

where $\varepsilon, \nu, \mathbb{E}$ are circuit parameters and K is the coupling constant with the other node. This voltage is used to calculate $C_j(t)$ since it is part of the Hamiltonian described in Eq. 3.8. Note that the last term in Eq. 3.10 has a term $U_{NL,3-j}$. This indicates the coupling from node j to node $3-j$, effectively indicating the connection between node 1 and 2 for $j = 1$ and between node 2 and node 1 for $j = 2$.

By experimentally disconnecting the circuit, one should take $C_j(t) = 0$ in the suggested model. Since we are interested in the existence of synchronisation in any scenario, including the scenario where $C_j = 0$, this will be explained in more detail in a later section.

Since both systems have an interaction via the electrical circuit which was covered by H_{ej}, we still need to define the interaction through the phonon interaction by tunnelling. This Hamiltonian is given by

$$H_{int} = -\mu(b_1^\dagger b_2 + b_2^\dagger b_1) \tag{3.11}$$

where μ is the intensity of this coupling. [10] Notice that Eq. 3.11 is symmetric, which implies that the quantum interaction will always be symmetric. This is opposite to the classical coupling of the electricity $U_{NL,j}$ which can be directed just as the networks in the previous chapter. More details will be given about these interactions in the section about the quantum network.

After reviewing all three components of Eq. 3.5 extensively, we may write down the total Hamiltonian explicitly:

$$\begin{aligned} H = \sum_{j=1,2} \Bigg(&- \Delta_j a_j^\dagger a_j + \omega_{mj}\left[1 + \frac{C_j(t)}{2}\right] b_j^\dagger b_j - g a_j^\dagger a_j (b_j^\dagger + b_j) + iE(a_j^\dagger - a_j) \\ &+ \frac{\omega_{mj}}{4} C_j(t)(b_j^\dagger b_j^\dagger + b_j b_j)\Bigg) - \mu(b_1^\dagger b_2 + b_2^\dagger b_1) \end{aligned} \tag{3.12}$$

which forms, together with Eqs. 3.9, 3.10 and the initial conditions, the complete theory of two connected optomechanical systems.

3.2 The two-system model

In this section we will examine the exact dynamics and synchronisation conditions for two coupled optomechanical systems. Due to the ability to calculate the information transfer analytically, the two-system model will be investigated first. Furthermore, the complex interaction between all nodes will exponentially increase the difficulty of the problem.

3.2.1 Synchronisation

Synchronisation in the quantum domain originates from the idea that information needs to be transferred. Although various applications using qubits are being examined at the moment, the suggested network could also work in this context of a continuous variable system which was discussed in the previous section. The continuous variables are the earlier introduced a and b. By linking two nodes, the wave function of the two nodes, which are time-independent since we are in the Heisenberg picture, remain constant but the product of the Hamiltonian and the wave functions will gradually become the same. Effectively, we could say the information contained in node 1 is then the same as in node 2, so we transferred information. Just as in the

classical scenario, we are interested to find out the existence of synchronisation.

In order to quantify this for the quantum mechanical system, we will look into the difference in quantum operators for both systems.

$$\hat{q}_- = \hat{q}_1 - \hat{q}_2 \tag{3.13}$$
$$\hat{p}_- = \hat{p}_1 - \hat{p}_2 \tag{3.14}$$

Whenever both $\hat{p}_-$ and $\hat{q}_-$ vanish asymptotically to zero, the system stabilises. Another useful measure for being in a synchronous state was first derived by Mari et al. [10]

$$S_c(t) = \langle \hat{q}_-(t)^2 + \hat{p}_-(t)^2 \rangle^{-1} \leq 1 \tag{3.15}$$

Notice that in the classical situation at full synchronisation, S_c tends to infinity. Quantum mechanically this is impossible, since the Heisenberg uncertainty tells us that both position and momentum of the same system cannot be measured with an infinite precision. We therefore find that S_c is bounded above by 1.

In order to quantify the function above to a more meaningful extend, we write a_j in terms of its expectation value and the perturbation. We denote

$$a_j(t) = A_j(t) + \delta a_j(t) \tag{3.16}$$

where $A_j(t) = \langle a_j(t) \rangle$ is the average and $\delta a_j(t)$ is the perturbation around the average. In the same manner we define $B_j(t)$, $\delta b_j(t)$, $P_j(t)$, $\delta p_j(t)$ and $Q_j(t)$, $\delta q_j(t)$. The useful aspect of this split up is that we have created two divisions. We introduced a semi-classical synchronisation in terms of the expectation value, which is described as

$$\langle \hat{q}_- \rangle = \langle \hat{q}_1 \rangle - \langle \hat{q}_2 \rangle = Re[B_1(t)] - Re[B_2(t)] \tag{3.17}$$
$$\langle \hat{p}_- \rangle = \langle \hat{p}_1 \rangle - \langle \hat{p}_2 \rangle = Im[B_1(t)] - Im[B_2(t)] \tag{3.18}$$

Secondly, for the perturbation, the same measurement can be prescribed

$$\delta\hat{q}_- = \delta\hat{q}_1 - \delta\hat{q}_2 = Re[\delta b_1(t)] - Re[\delta b_2(t)] \tag{3.19}$$
$$\delta\hat{p}_- = \delta\hat{p}_1 - \delta\hat{p}_2 = Im[\delta b_1(t)] - Im[\delta b_2(t)] \tag{3.20}$$

Note that the last measure is not mentioned by Mari et. al, but I will return to this statement in one of the proceeding sections.

Explicit calculation of the average synchronisation measure is rather simple if we have an equation for $B_1(t)$ and $B_2(t)$. This will be covered in the next section.

3.2.2 Derivation of the equations of evolution

Now all methods of synchronisation are explained, we may start deducing the equations of motion for the optomechanical systems shown in Figure 9. Consider the time-dependent Hamiltonian of Eq. 3.12. Converting this formula into the evolution equations of the operators is described by Scully and Zubairy in their book Quantum optics. [14] Together with the formulation of the optical bath formulated by Gardiner and Collett [6], the general solution of any optical quantum system interacting with an optical bath is given by

$$\dot{o_j} = \frac{i}{\hbar}[H, o_j] - \kappa o_j + \sqrt{2\kappa}\, o_j^{in}(t), \quad o \in \{a, b\} \tag{3.21}$$

where κ is the damping coefficient and $o_j^{in}(t)$ is the input bath operator belonging to the system. The latter can best be regarded as the interaction between the optomechanical system and its environment, which is

actually considered noise in the system. $o_j^{in}(t)$ can be modelled as zero-mean white noise with variance 1, and is uncorrelated for all nodes and times, that is

$$\langle a_j^{in}(t)^\dagger a_{j'}^{in}(t') + a_{j'}^{in}(t') a_j^{in}(t)^\dagger \rangle = \delta_{jj'}\delta(t-t') \tag{3.22}$$

$$\langle b_j^{in}(t)^\dagger b_{j'}^{in}(t') + b_{j'}^{in}(t') b_j^{in}(t)^\dagger \rangle = (2n_b+1)\delta_{jj'}\delta(t-t') \tag{3.23}$$

where n_b is the Boltzmann number given by $n_b = [\exp(\frac{\hbar\omega_j}{k_B T}) - 1]^{-1}$. Here k_B is the Boltzmann constant and T the temperature in the cavity. Since both ω_j are almost the same, n_b can as well be taken constant for both systems. [6]

Now filling in Eq. 3.12 into Eq. 3.21 yields the following equations for the annihilation operators a_j and b_j:

$$\dot{a_j} = [-\kappa + i\Delta_j + ig(b_j + b_j^\dagger)]a_j + E + \sqrt{2\kappa}\, a_j^{in} \tag{3.24}$$

$$\dot{b_j} = \left(-\gamma + i\omega_{mj}\left[1 + \frac{C_j(t)}{2}\right]\right) b_j + iga_j^\dagger a_j + i\mu b_{3-j} - i\frac{\omega_{mj}}{2} C_j(t) b_j^\dagger + \sqrt{2\gamma}\, b_j^{in} \tag{3.25}$$

which govern, together with a given set of initial conditions, the time-evolution of the position and momentum operators.

As explained in the previous section, it is interesting to know what the evolution is when the system is approximated using the average-perturbation method given in Eq. 3.16. We may apply this directly to Eqs. 3.24 and 3.25 such that the following set of equations holds for the average operators.

$$\dot{A}_j = [-\kappa + i\Delta_j + ig(B_j + B_j^*)]A_j + E \tag{3.26}$$

$$\dot{B}_j = \left(-\gamma + i\omega_{mj}\left[1 + \frac{C_j(t)}{2}\right]\right) B_j + igA_j^* A_j + i\mu B_{3-j} - i\frac{\omega_{mj}}{2} C_j(t) B_j^* \tag{3.27}$$

Notice that the average only contains deterministic values; a given set of initial conditions and the equations fully determine the behaviour in time. When looking at the evolution of the perturbed operators, this is different.

$$\dot{\delta a_j} = [-\kappa + i\Delta_j + ig(B_j + B_j^*)]\delta a_j + igA_j(\delta b_j^\dagger + \delta b_j) + \sqrt{2\kappa}\, a_j^{in} \tag{3.28}$$

$$\dot{\delta b_j} = \left(-\gamma + i\omega_{mj}\left[1 + \frac{C_j(t)}{2}\right]\right) \delta b_j + igA_j^* \delta a_j + igA_j \delta a_j^\dagger + i\mu\delta b_{3-j} - i\frac{\omega_{mj}}{2} C_j(t)\delta b_j^\dagger + \sqrt{2\gamma}\, b_j^{in} \tag{3.29}$$

The bath operators a_j^{in}, b_j^{in} are modelled stochastically, so the given initial conditions cannot fully determine its behaviour to due quantum noise. To avoid using too complicated expressions and since the perturbation is always small, the differential equations above were linearised in δa_j and δb_j. Using advanced mathematical (stochastic) calculus an analytical result could be derived, however, the synchronisation conditions are so complex so it's better to just analyse the behaviour right away.

3.2.3 Synchronisation measures

After examining the equations of motion in the previous section, the synchronisation measure introduced in Eq. 3.17 has now been classified. Although the method described works in a semi-classical environment, a pure quantum phenomenon cannot be explained. This is because the synchronisation which took place is only synchronisation in average, and not complete synchronisation. We require a more advanced measure, which will be examined now.

Analogue to the general synchronisation condition (recall Eq. 3.15), one may define a pure quantum synchronisation measure as follows

$$S_c'(t) = \langle \delta q_-^2(t) + \delta p_-^2(t) \rangle^{-1} \tag{3.30}$$

The measure described does contain quantum information only, but is hard to use in practice. We therefore require the system always to be in a Gaussian state. A *Gaussian state* is a ground state of a Hamiltonian

which is quadratic in the creation and annihilation operators. In practice, this means that the linearisation of the quantum operators δa_j and δb_j is justified. Moreover, the measure $S_c'(t)$ can be written in terms of correlations between the perturbation operators. [9]

The definitions of a_j and b_j introduced in the first section of this chapter can be rewritten such that $\hat{x}, \hat{y}, \hat{p}, \hat{q}$ are functions of $a, a^\dagger, b, b^\dagger$ only. This yields

$$\begin{aligned} \hat{x}_j &= \frac{1}{\sqrt{2}}(a_j^\dagger + a_j), \quad \hat{y}_j = \frac{i}{\sqrt{2}}(a_j^\dagger - a_j) \\ \hat{q}_j &= \frac{1}{\sqrt{2}}(b_j^\dagger + b_j), \quad \hat{p}_j = \frac{i}{\sqrt{2}}(b_j^\dagger - b_j) \end{aligned} \tag{3.31}$$

Introducing the vector $\hat{\mathbf{u}} = (\delta x_1, \delta y_1, \delta x_2, \delta y_2, \delta q_1, \delta p_1, \delta q_2, \delta p_2)^T$ and $\hat{\xi} = (\hat{x}_1^{in}, \hat{y}_1^{in}, \hat{x}_2^{in}, \hat{y}_2^{in}, \hat{q}_1^{in}, \hat{p}_1^{in}, \hat{q}_2^{in}, \hat{p}_2^{in})^T$, we may write the equations of motion (Eqs. 3.28 and 3.29) in a much shorter form

$$\frac{\partial \hat{\mathbf{u}}}{\partial t} = \mathbf{S}\,\hat{\mathbf{u}} + \hat{\xi} \tag{3.32}$$

where $\hat{\mathbf{u}}$ is the evolution of the perturbations in time, S is a matrix which can be deduced directly from Eqs. 3.28 and 3.29 and $\hat{\xi}$ contains the input (noise) from the environment. See Appendix 5 for a more complete overview of the matrix $\mathbf{S}$. Now consider the symmetric covariance matrix $\mathbf{V}$ defined as

$$V_{ij}(t) = V_{ji}(t) = \frac{1}{2}\langle \hat{u}_i(t)\hat{u}_j(t) + \hat{u}_j(t)\hat{u}_i(t)\rangle \tag{3.33}$$

which evolves in time as

$$\frac{\partial \mathbf{V}}{\partial t} = \mathbf{S}\mathbf{V} + \mathbf{V}\mathbf{S}^T + \mathbf{N} \tag{3.34}$$

where $\mathbf{S}$ is the earlier mentioned matrix and $\mathbf{N}$ is a noise correlation matrix of $\hat{\xi}$, which is diagonal and is uncorrelated with itself for all times. [9]

Now we may construct the synchronisation measure S_c' in terms of the covariance matrix $\mathbf{V}$, which is [9]

$$S_c'(t) = \left(\frac{1}{2}(V_{55}(t) + V_{77}(t) - 2V_{57}(t) + V_{66}(t) + V_{88}(t) - 2V_{68}(t))\right)^{-1} \tag{3.35}$$

Now we introduce another measure, called the quantum fidelity, [8] which can be calculated directly from the covariance matrix $\mathbf{V}$ for Gaussian states:

$$\mathcal{F} = \frac{2}{\sqrt{\Lambda + \lambda} - \sqrt{\lambda}} \exp\left[-\beta^T(\mathbf{V}_1 + \mathbf{V}_2)^{-1}\beta\right] \tag{3.36}$$

where

$$\mathbf{V}_1 = \begin{pmatrix} V_{11} & V_{12} \\ V_{21} & V_{22} \end{pmatrix}, \quad \mathbf{V}_2 = \begin{pmatrix} V_{33} & V_{34} \\ V_{43} & V_{44} \end{pmatrix} \tag{3.37}$$

$$\beta = \sqrt{2}\begin{pmatrix} Re[A_1] - Re[A_2] \\ Im[A_1] - Im[A_2] \end{pmatrix} \tag{3.38}$$

$$\Lambda = \det(\mathbf{V}_1 + \mathbf{V}_2), \quad \lambda = (\det(\mathbf{V}_1) - 1)(\det(\mathbf{V}_2) - 1) \tag{3.39}$$

The quantum fidelity is a more advanced method to value the degree of synchronisation in the quantum regime. The allowed values for $\mathcal{F}$ are between 0 (no overlap in wave functions) and 1 (systems are completely synchronised). In order for synchronisation to take place, we require $\mathcal{F}$ to asymptotically grow to 1.

These are all required conditions to be able to investigate the behaviour of this system as time evolves. Now we are ready to investigate the results.

3.2.4 Results: the average

After deducing the equations of motion in the previous section, we can now plot the solutions as a function of time. We will first look into the average and thereafter at the perturbation.

In order to examine all aspects at once, the following plots were constructed by one evolution of Eqs. 3.26 and 3.27. All equations were integrated using the Euler forward method with a time step of $\Delta t = 0.005$. [15]

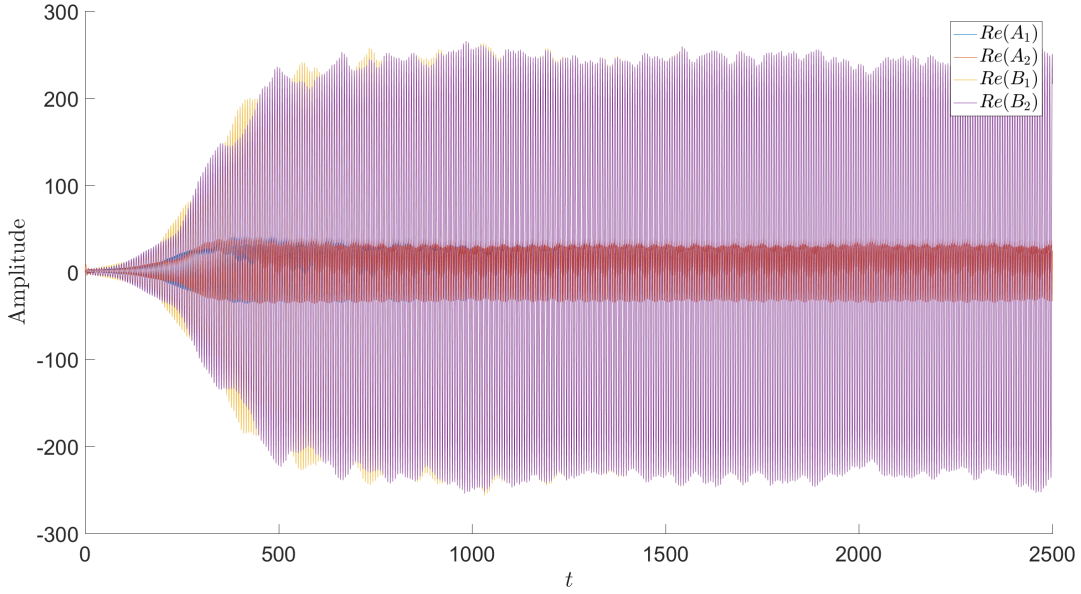

Figure 10: The evolution of the real part of the average operators A_j and B_j for the two coupled optomechanical systems. The following parameters were used: $\omega_{m1} = 1, \omega_{m2} = 1, \Delta_j = \omega_{mj}, g = 0.005, \kappa = 0.15, \gamma = 0.005, \eta = 0.01, \varepsilon = 0.18, \nu = 1, E = 10, \mathbb{E} = 26.7$. The coupling parameters are $K = 2$ and $\mu = 0.02$. For the initial conditions we have $A_1(0) = A_2(0) = 0$ (vacuum state) and $B_1(0), B_2(0)$ are random numbers with amplitude uniform between 0 and 1 and a uniformly chosen random phase. Also $U_{NL,1}(0), U_{NL,1}(0), \phi_0(0)$ and $\phi_1(0)$ are uniform random variables between 0 and 1.

Around $t = 0$, the values start to oscillate around 0. As time increases, the oscillations start to increase in amplitude until about $t = 500$. Here we are in a travelling wave state, which was discussed earlier in the classical situation. The colours yellow and blue are not visible for $t > 1000$ since they are almost equal to red and purple. Although this behaviour seems chaotic, this is no problem, since we require $\langle q_- \rangle$ and $\langle p_- \rangle$ to vanish to 0. Now extract the P_j and Q_j from the previous plot, which is shown below.

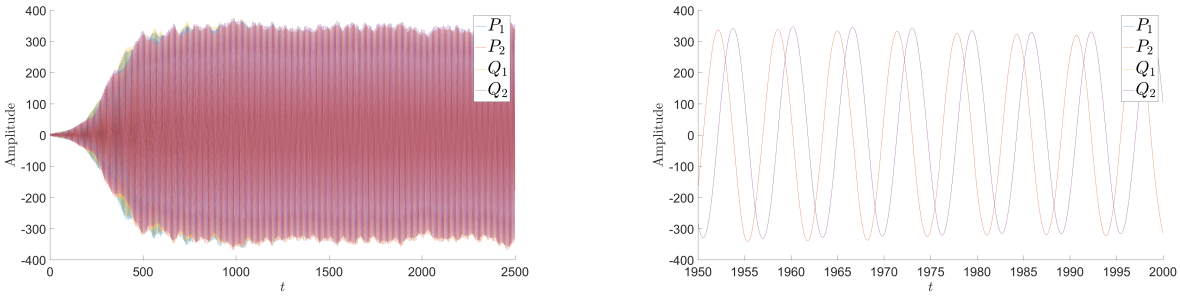

Figure 11: The evolution of the average momentum and position operators P_j and Q_j for the two coupled optomechanical systems. The parameters are the same as in the previous plot. The plot on the left side contains the whole domain and the right one is zoomed in between $t = 1975$ and $t = 2000$.

The plot shows the same behaviour as expected from the previous plot. Around $t = 500$ some slight colour difference are visible (so other colours than blue or red), but in the right plot they are invisible. This indicates that we may have found a solution which indeed vanishes to 0. This is shown in the next plot.

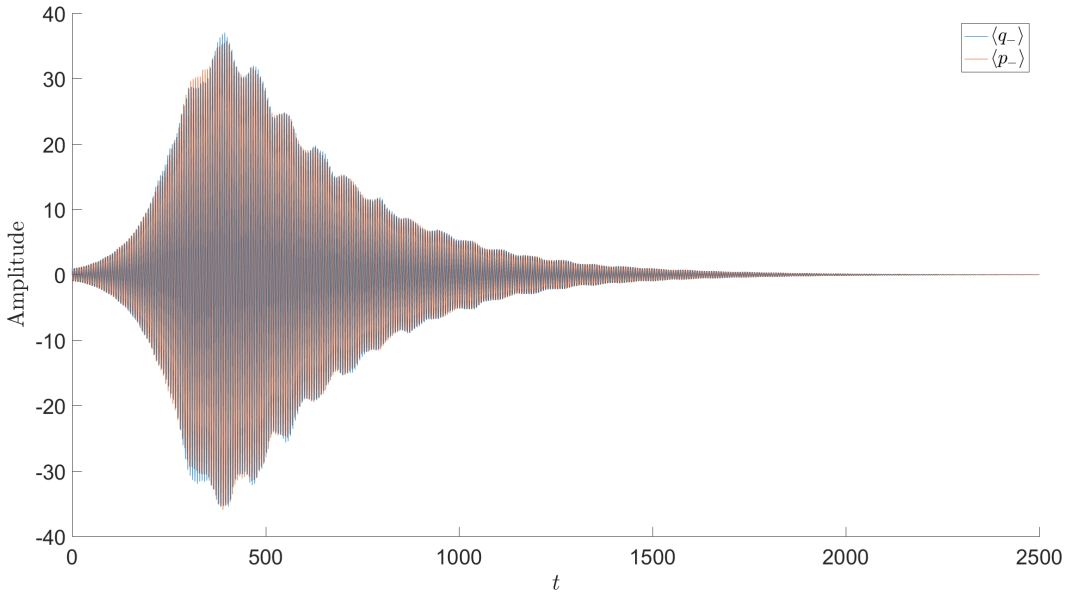

Figure 12: The evolution of the averages $\langle q_- \rangle$ and $\langle p_- \rangle$ for the two coupled optomechanical systems. The parameters are the same as in the previous plot. As required, the solution vanishes asymptotically with time.

This plot contains the classical synchronisation measures as calculated in Eqs. 3.17 and 3.18. As one might expect, this is indeed a valid situation where the difference between the averages vanishes asymptotically to zero. On the other hand, it's clear that this situation is not established in a direct way. It is required to create a large difference first, whereafter the difference vanishes again. This indicates that a small tweak in the setup of the two systems destabilises the whole situation, such that synchronisation no longer takes place. The following plot shows this behaviour.

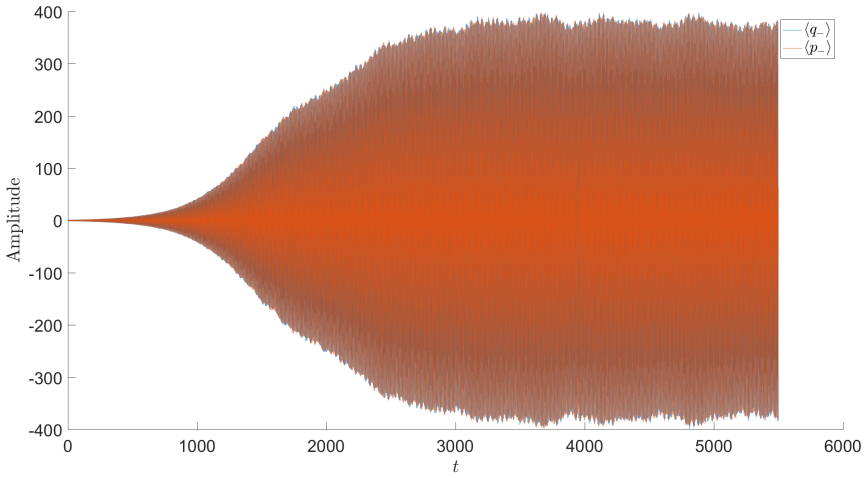

Figure 13: The evolution of the averages $\langle q_- \rangle$ and $\langle p_- \rangle$ for the two coupled optomechanical systems. The parameters are the same as in the previous plot, except that $E = 6$, which is 4 lower than before. As expected, the solution doesn't approach 0 as time increases.

The plot indicates that it is very important to tune the parameters used to generate a synchronisation in the average. Furthermore, it is interesting to note that the system described actually uses a double coupling, namely the classical coupling via the circuit (parameter K) and the quantum coupling via the gaseous interaction (parameter μ). By introducing the following plot, a comparison can be made to indicate whether synchronisation can take place when one of these connections is removed.

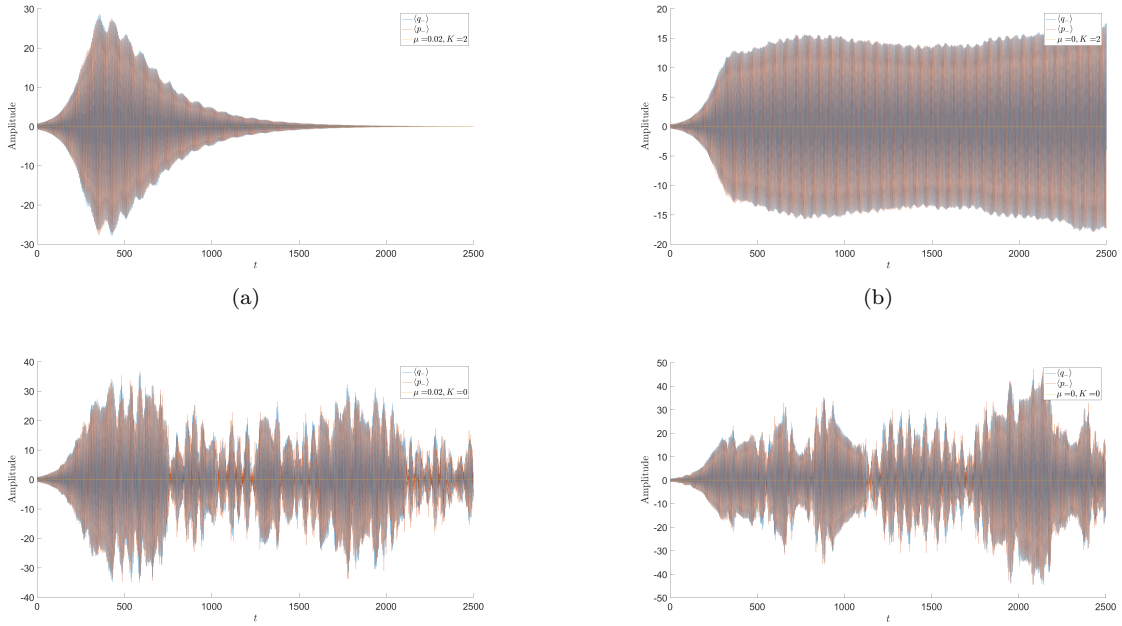

Figure 14: The evolution of the average synchronisation measures $\langle q_- \rangle$ and $\langle p_- \rangle$ for the two coupled optomechanical systems. The plots were constructed using a) both interactions, where b) only has a classical coupling, c) only has a quantum coupling and d) has no connection at all. Apart for this, all parameters are the same as previously mentioned.

By not coupling the two systems at all as shown in (d), synchronisation cannot take place. More interestingly, for both the existence of a solely classical coupling (b) or quantum coupling (c), the general idea doesn't hold. It is really required (for this set of parameters) to connect using both interactions to be able to synchronise. This conclusion is vital for the construction of the quantum network, so it will be extended upon in one of the later sections.

All examined figures are valid for synchronisation in average only. The following section will expand on the perturbation.

3.2.5 Results: the perturbation

After thoroughly examining synchronisation in the average, it is now time to look into the perturbation. The same procedure will be followed to hopefully generate the same results. The following plot was constructed by one simulation using Eqs. 3.28 and 3.29, but also Eqs. 3.26 and 3.27 for the averages were used.

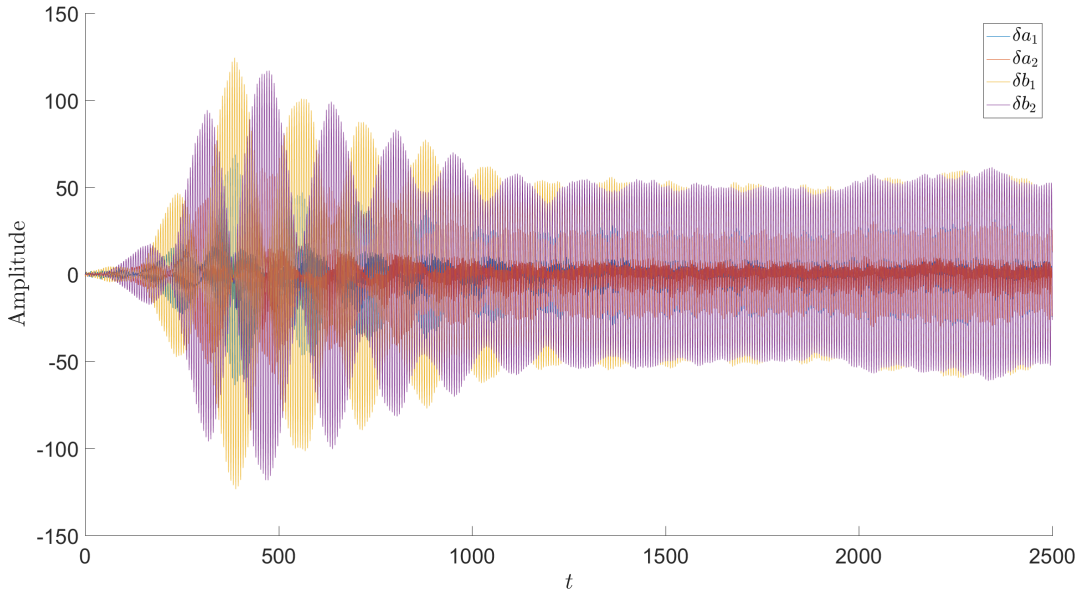

Figure 15: The evolution of the real part of the perturbation operators δa_j and δb_j for the two coupled optomechanical systems. The following parameters were used: $\omega_{m1} = 1, \omega_{m2} = 1, \Delta_j = \omega_{mj}, g = 0.005, \kappa = 0.15, \gamma = 0.005, \eta = 0.01, \varepsilon = 0.18, \nu = 1, E = 10, \mathbb{E} = 26.7$. The coupling parameters are $K = 2$ and $\mu = 0.02$.As initial conditions we have $A_1(0) = A_2(0) = 0$ (vacuum state) and $B_1(0), B_2(0), \delta a_1(0), \delta a_2(0), \delta b_1(0), \delta b_2(0)$ are random numbers with amplitude uniform between 0 and 1 and a uniformly chosen random phase. Also $U_{NL,1}(0), U_{NL,1}(0), \phi_0(0)$ and $\phi_1(0)$ are uniform random variables between 0 and 1.

Comparing this figure with Figure 10, there are some similarities and differences visible. First of all, the plot starts with rapid oscillations which gradually increase in amplitude until $t = 500$. By then, the amplitude slowly drops to a non-zero amplitude. This is in contrast to the previous plot where the amplitude of the variables did not show this behaviour and instead remained high. Furthermore, the difference between the variables is much better visible, since both red, blue and yellow are visible, indicating that quantum synchronisation is not quite achieved.

These issues indicate that perturbation quantum synchronisation will not be achieved so easily. Now the physical variables $\delta p, \delta q$ will be examined.

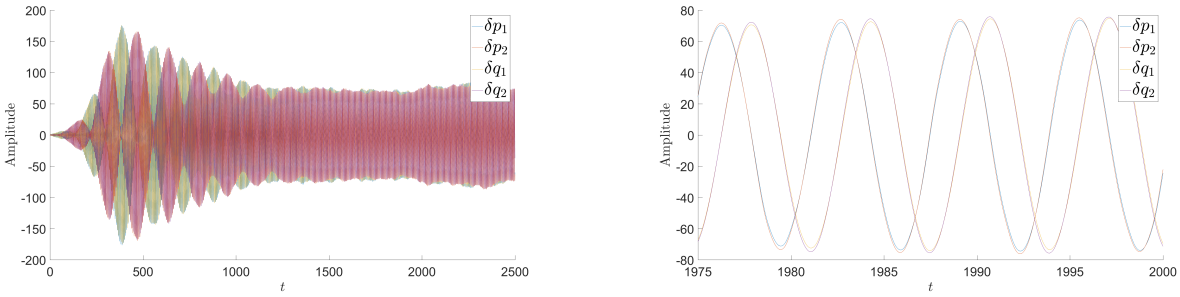

Figure 16: The evolution of the perturbation momentum and position operators δp_j and δq_j for the two coupled optomechanical systems. The parameters are the same as in the previous plot. The plot on the left side contains the whole domain and the right one is zoomed in between $t = 1975$ and $t = 2000$.

Comparing this plot to the previous, the resemblance is clear. At first, a vast increase in amplitude is visible for the rapid oscillations. After a certain moment in time, the solution stabilises and then slowly decays. However, here a certain fluctuation (due to quantum noise) is still present. Looking at the right plot, quantum synchronisation doesn't seem to be complete just yet, nor we can conclude that it will ever happen. It is therefore required to look at the following plot.

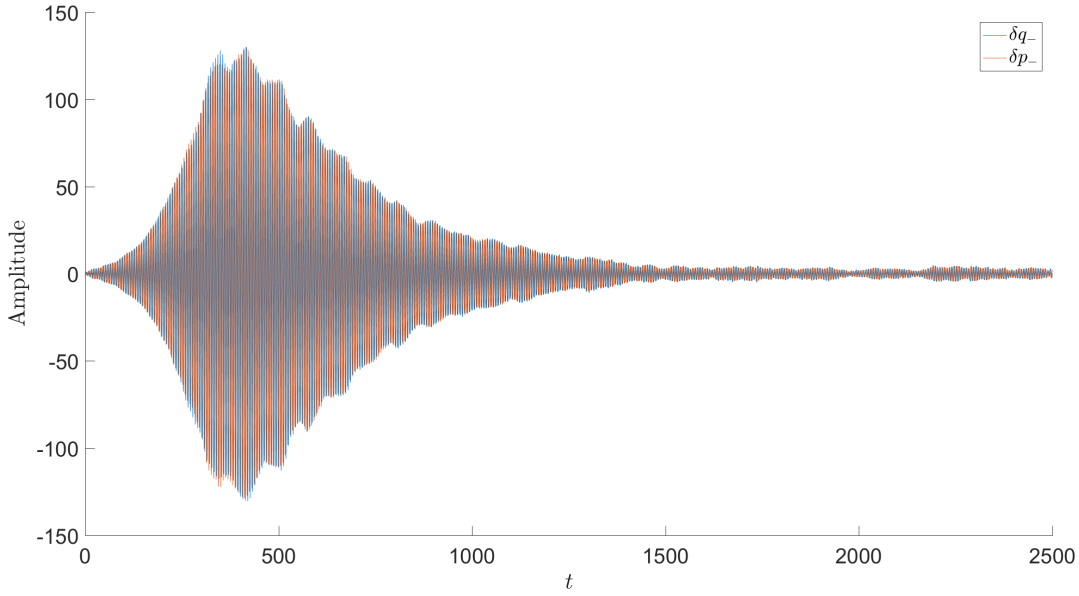

Figure 17: The evolution of the perturbation quantifiers δq_- and δp_- for the two coupled optomechanical systems. The parameters are the same as in the previous plot. The plot does not converge to zero due to the high intensity of the noise.

This is the plot of the equations presented in Eqs. 3.19 and 3.20. Here the true nature of the problem suggested with this method becomes clear: as t increases after $t = 1500$, it cannot be concluded from this plot whether the synchronisation really improves any further. This is in contrast to Figure 12, where synchronisation in the average continues to improve as t increases.

It is clear that this plot is the noisiest plot until now. Although one can try averaging over a certain number of simulations to reduce noise, this is not helpful enough. The amplitude of the oscillations around $t = 500$ will drop, but the plot will remain noisy. In order to visualize this, the following plot conveys my argument.

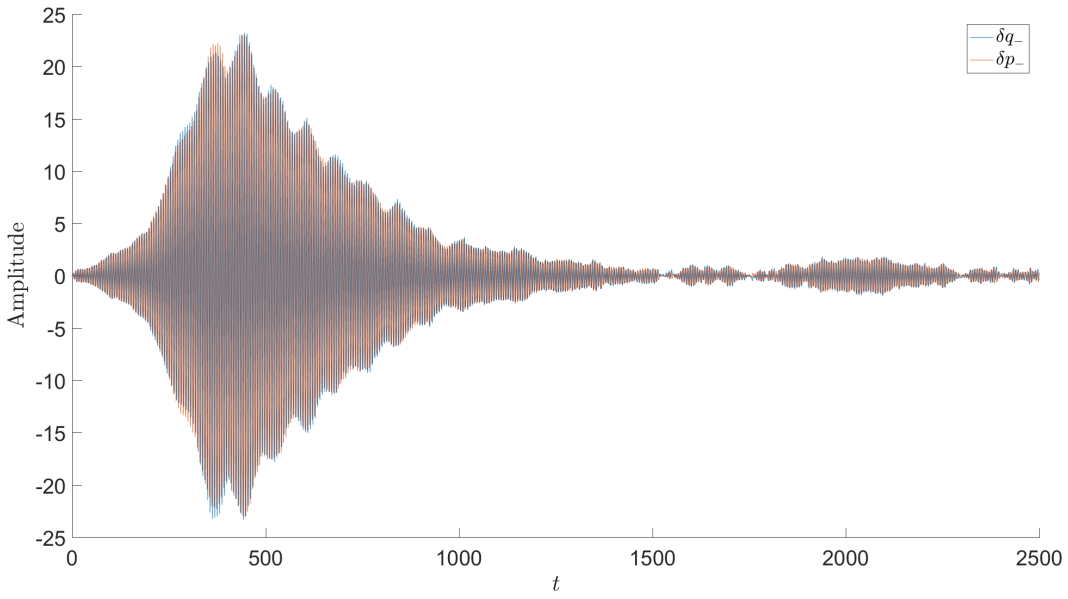

Figure 18: The evolution of the perturbation momentum and position operators δp_- and δq_- for the two coupled optomechanical systems. The plot contains an averaged value over 10 simulations.

At first glance, nothing changed. However, on close observation, the amplitude on the vertical axis has dropped heavily. This is because of the averaging over 10 simulations, where the individual evaluations cancelled each other out. However, for $t > 1500$, the observation is quite similar to in the previous plot. Due to quantum noise, several oscillations are visible which never seem to cancel out. However, this is not necessarily a problem. The plotted measure in Figure 17 is not a genuine quantum measure, but rather a measure to gain inside into the difficult matter of quantum synchronisation.

The same plot can be constructed for $S_c'(t)$, which is a genuine quantum measures introduced by Mari et. al. [10]

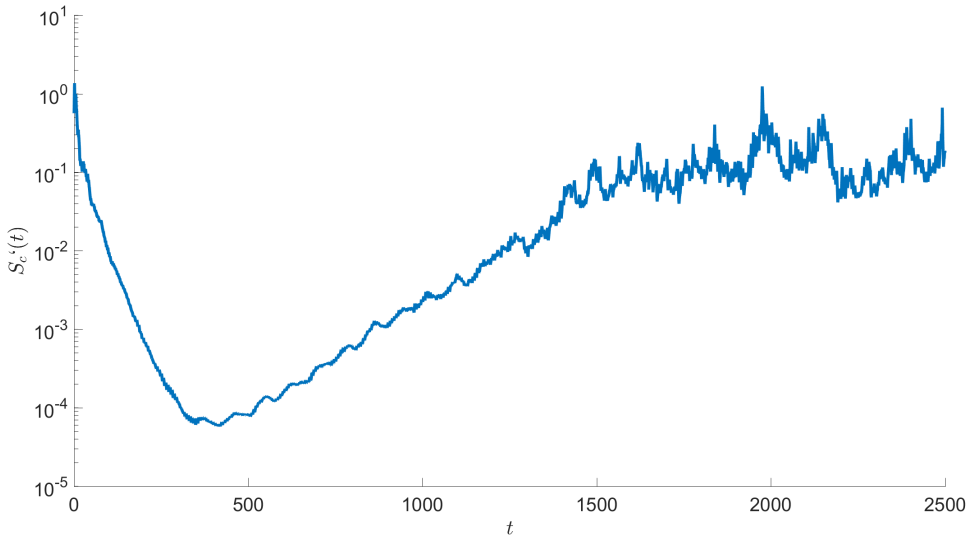

Figure 19: The evolution of the quantum synchronisation measure $S_c'(t)$ for the two coupled optomechanical systems. The vertical axis is a logarithmic axis.

The evolution of this quantum synchronisation measure is rather extraordinary. The first part of the graph ($t < 500$) is in compliance with Figure 12; both graphs show a deviation from the synchronous state. From this point on, the classical solution now only approaches the synchronisation moment even more. The quantum synchronisation does the same, up to a certain moment. This is around $t = 1200$. From here, the quantum noise takes the upper hand, effectively making a classical synchronisation impossible. This effect was also recognised by Li, Li and Song. [9] Fortunately, this is not the end of the story. The true quantum information is hidden in the total Hamiltonian and wave function. The earlier introduced fidelity $\mathcal{F}$ is a measure of the overlap in wave function, effectively making it more a quantum measure than any of the other measures. The following plot was constructed.

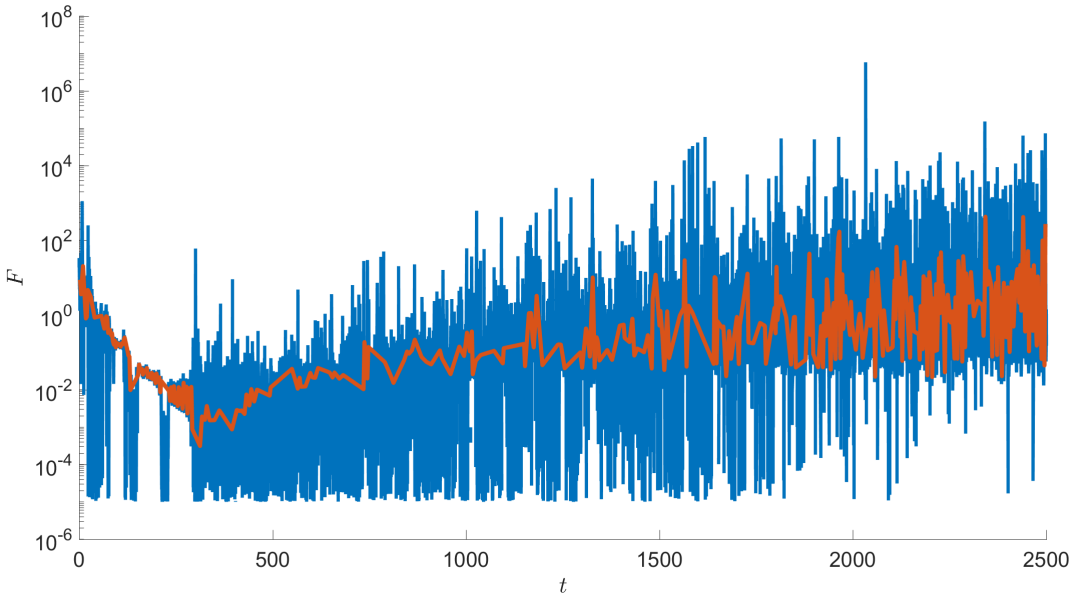

Figure 20: The evolution of the quantum synchronisation measure $\mathcal{F}$ for the two coupled optomechanical systems. The vertical axis is a logarithmic axis. The orange line shows the fidelity averaged over 500 time steps.

The plot above shows the genuine (random) quantum effects introduced in the model. The blue lines change drastically as a function of time, that's why the average over 500 time steps is shown in orange. Unfortunately, this doesn't improve the figure much. The same chaos was expected by Li, Li and Song, but the amplitude is not in compliance with their results. [9]

The physical interpretation of the fidelity is that it is a measure between 0 (no overlap) and 1 (same wave function) between the two wave functions of the two connected systems. The graph above can therefore not be a physical one since the amplitude exceeds 1 by far, and further discussion on this matter will be handled in the discussion near the end of the report. A lot more can be said about this intriguing subject, but in order to utilise this theory for anything useful, we will look into the quantum network.

3.3 Quantum network

After thoroughly analysing the equations of motion for two coupled systems, it is time to expand this two-system model into a network structure. We will denote the network structure again by the adjacency matrix. In the general Hamiltonian shown by Eq. 3.12, the interaction between two systems is always symmetric, thus the interaction strength from 1 to 2 is the same as 2 to 1, for both the electrical connection via parameter K and the gaseous interaction via parameter μ. Since we have two different (possible) networks, we will make a distinction between the classical network $\mathbf{A}_c$ and the quantum network $\mathbf{A}_q$.

Generalising the Hamiltonian to the general network is straight-forward. Recall that the Hamiltonian of a node j in the rotating-wave approximation is given as

$$H_j = -\Delta_j a_j^\dagger a_j + \omega_{mj}\left[1 + \frac{C_j(t)}{2}\right] b_j^\dagger b_j - g a_j^\dagger a_j (b_j^\dagger + b_j) + iE(a_j^\dagger - a_j) + \frac{\omega_{mj}}{4} C_j(t)(b_j^\dagger b_j^\dagger + b_j b_j) \tag{3.40}$$

and the gaseous interaction between nodes i and j as

$$H_{ij} = H_{ji} = -\mu A_{q,ij}(b_i^\dagger b_j + b_j^\dagger b_i) \tag{3.41}$$

where $A_{q,ij}$ has the value 1 when the link between node i and j is present and 0 otherwise. Since the last equation is symmetric, the adjacency matrix $\mathbf{A}_q$ will be too. Now the total Hamiltonian of a network of optomechanical systems can be computed

$$H = \sum_{j=1}^{n} H_j + \sum_{i \neq j} H_{ij} \tag{3.42}$$

where H_j is the Hamiltonian of optomechanical system j and H_{ij} is the interaction Hamiltonian. The equations for the j'th Duffing circuit change to

$$\frac{d}{dt}\phi_j = U_{NL,j} \tag{3.43}$$

$$\frac{d}{dt}U_{NL,j} = -\varepsilon U_{NL,j} - \phi_j - \nu\phi_j^3 + \mathbb{E}\cos(\omega_0 t) + \varepsilon K \sum_{i \neq j} A_{c,ij}(U_{NL,i} - U_{NL,j}) \tag{3.44}$$

where $A_{c,ij}$ is the classical adjacency matrix which has value 1 when a connection exists between nodes i and j and 0 otherwise. From now on, all connected optomechanical systems will simply be called nodes, and the interaction between the nodes are called links.

After applying the same strategy as in the previous section, all equations of motion of the averages and the perturbations can be obtained. There are $6n$ equations which can be extracted as $10n$ physical variables. Naturally this cannot be analysed for an arbitrarily chosen n and for arbitrary network structures, so we will look into some specific examples.

3.3.1 Return to the classical network

In this section the classical ring network from the classical network is reused. In this ring, 7 nodes are connected to their two nearest neighbours forming a circle (see Figure 1). Now assume both the classical and quantum network are alike and equal to this ring network, effectively taking $\mathbf{A}_c = \mathbf{A}_q = \mathbf{A}$. Furthermore, assume $\delta = 0$ such that the network is completely symmetrical. We wish to identify the synchronisation between all nodes, however, this is not possible. It would be required to invent a measure which effectively measures the wave function overlap between (in general) n functions. This would not only be hard, it is also not necessary. Since we adopt this network to invent a quantum network in which information can be transferred, we do not require it to send information to every node in the network, but only to a single one. When accessing the internet, when you are searching for an internet page, not everyone on the internet requires to have the exact same page before you are able to see it. Therefore the measures discussed in the previous section are still usable. The generalisation of the synchronisation measures from nodes 1 and 2 to nodes i and j is trivial, so we can proceed to the results right away.

Since the ring network is circular and symmetric, no specific start node can be chosen. It is interesting to examine the results between neighbouring and non-neighbouring nodes. The following figure shows the classical synchronisation measure q_- for different combinations of nodes. The plot for p_- is not included since it exhibits quantitatively the same effect.

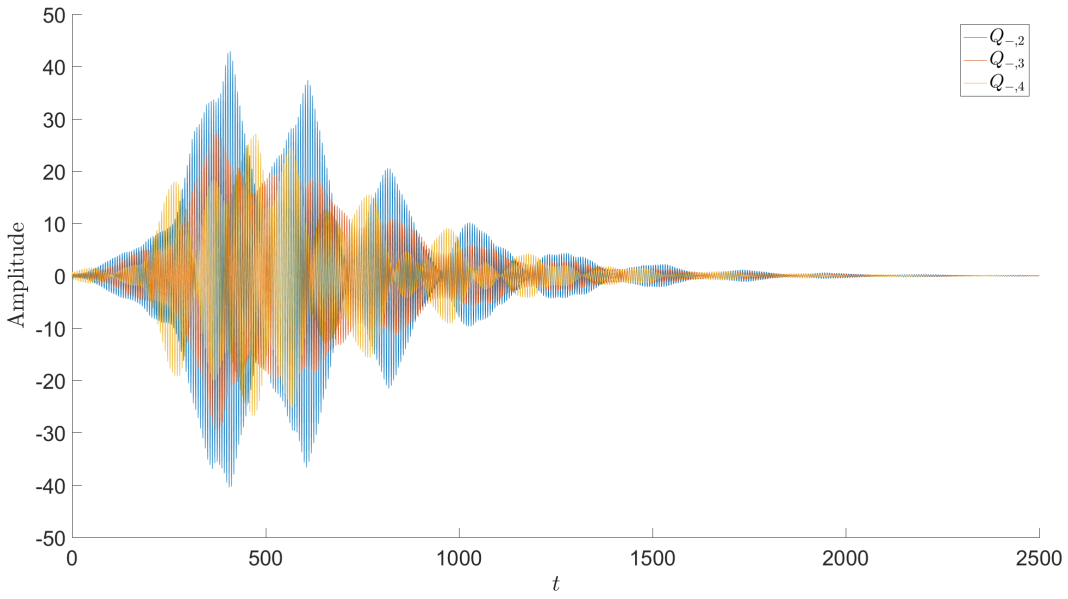

Figure 21: The evolution of the classical synchronisation measure $\langle q_- \rangle$ for the ring network. The plot consists of three lines: the difference between node 1 and 2 (blue), node 1 and 3 (red) and node 1 and 4 (yellow). All parameters are the same as before.

The plot shows that the classical synchronisation measure $\langle q_- \rangle$ indeed tends to zero for all connections from node 1 to nodes 2, 3 and 4 (the ring is symmetric and nodes 5,6,7 will be therefore show the same result). This means actual synchronisation can appear between node 1 and the other nodes. Furthermore, it is expected that node 2 will be synchronised earlier than node 4, simply because node 2 is closer to node 1 than node 4 is. By inspecting the figure above, this conclusion does not hold. The nodes in the network are in turn the most synchronised, indicating that the network converges as a whole rather than a local area only. This principle might be regarded as useful, but it is not in this context. A quantum internet has several connections and several tasks to perform at the same time. Synchronising with more nodes requires the network to use a larger time, which is not preferable.

The network proposed is therefore not ideal to be used as a quantum internet. The following section will propose another solution.

3.3.2 Quantum internet

Although no cut-and-clear network has been invented when regarding the future quantum internet, several ideas were proposed to model this. I will follow the path of the small-world quantum network explained by Li, Li and Song. [9]

The basics of this network consists of a ring network of n main nodes which are coupled to each other symmetrically in a classical way. This structure could resemble a set of handlers which transfer your information to them over a certain distance, to another node from where it is brought to the actual receiver. The nodes from the ring network more act like transferrers than all other nodes. Data centres actually work in the same way. Larger companies like Google even built their own data centre in the Netherlands to ensure a stable communication flow for all their services for a large part of Europe. [13] The general idea is that your computer connects to a data centre, which connects you again to the source you wish. This is exactly the principle of the nodes in the ring structure.

The users of the quantum internet are generally connected to one ring network node, which will be called main nodes. A user is called a sub node. The user requires a strong connection, therefore, as examined in one of the previous sections, both a classical and a quantum link are required to synchronise with a main node. Naturally, not all users connect to the same node, so in order to transfer information, the information has to pass a few main nodes before it reaches the target node.

This process is not ideal. Apart from that, no quantum links are available in the ring network, so actual synchronisation is not possible at all now, only between sub node and main node but that is not what we aim for. We therefore require a node which is capable of making a connection to another by temporarily adding a quantum link between the main nodes in the circuit. Since the network is used on and off, those linkings might as well be modelled as if they happen stochastically with a chance of connection of $P = 0.1$. Naturally, while modelling this property, it is vital to verify that a direct quantum link is available between the main node of the emitter node and the main node of the receiver node.

The constructed network fulfils the main requirements for the network to function. The network forms a small world network, where starting from a node, all other nodes can be reached by travelling over only a few lines. More discussion and information about the small world network can be found in Appendix 6.

The following figure shows an example of the proposed network structure.

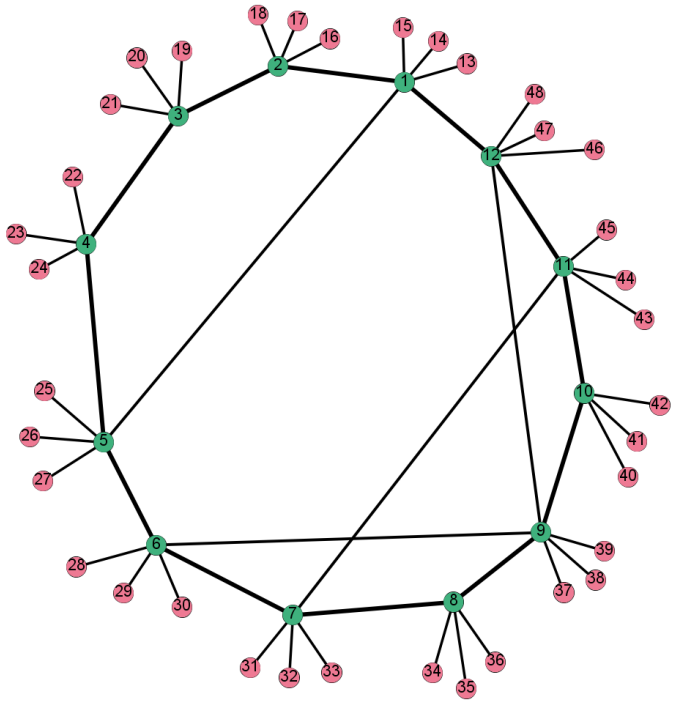

Figure 22: Schematic representation of the constructed quantum network. The green nodes coupled by the thick black lines are the main nodes which form a classical ring network. The outer nodes coloured in pink are the sub nodes which are connected by thin lines to a main node. These sub nodes are connected using both classical and quantum links. Random quantum links are present as well, for example between node 1 and 5. They are present with a chance of $P = 0.1$.

It is important to distinguish the three possible interactions. The thick lines indicate a pure classical coupling filling the coupling matrix $\mathbf{A}_c$. The medium sized-lines between the green nodes in the middle of the figure are coupled quantum mechanically belonging to adjacency matrix $\mathbf{A}_q$. Furthermore, the thinnest lines have

both a classical and quantum coupling and are therefore visible in both matrices.

As mentioned before, we would like to investigate the possibility of synchronisation. As usual this is done numerically. In order to save computation time, only the classical synchronisation measure is examined from node 13.

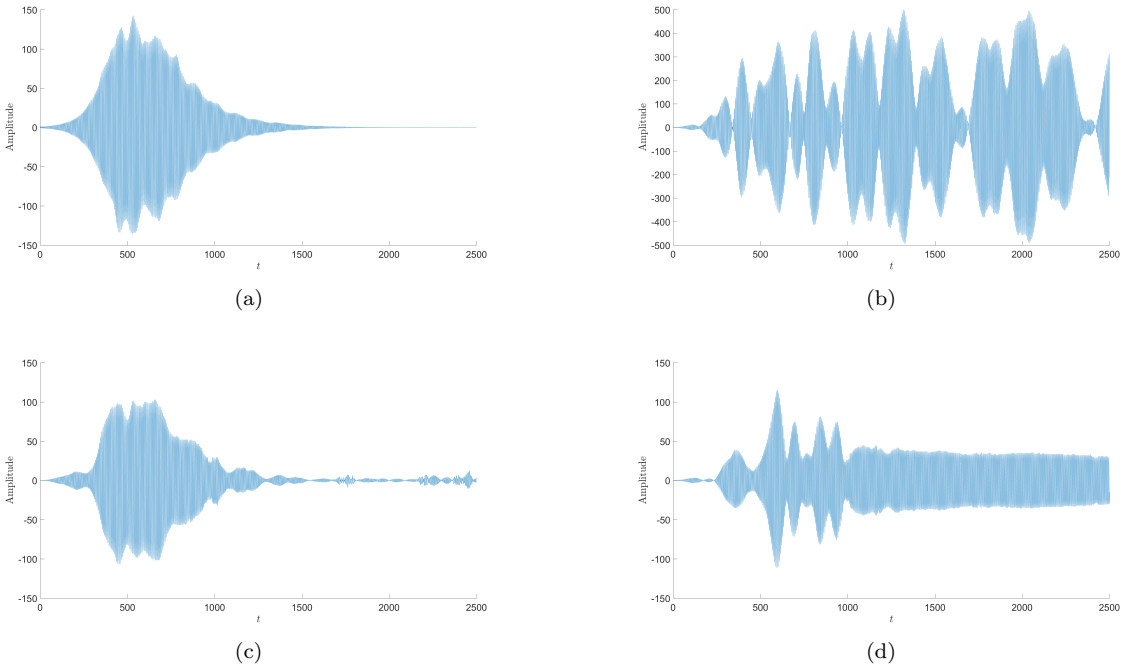

Figure 23: The evolution of the average $\langle q_- \rangle$ for the small world network of coupled optomechanical systems. The coupling parameters are $K = 5$ for the ring network and $K = 10$ for the connection between main and sub nodes. Furthermore, $\mu = 0.02$. All other parameters are the same as before. The network structure used is shown in Figure 22. The plot show the connection between (a) node 13 and 14 (same main node), (b) node 13 and 16 (classical ring coupling), (c) node 13 and 25 (quantum coupling) and (d) node 13 and 45 (no coupling).

The collection of graphs shown in Figure 23 shows the evolution for the synchronisation measure $\langle q_- \rangle$ for four different connections. In (a), the connection between node 13 and 14 is explored. Both sub nodes are connected to main node 1, see Figure 22. As expected due to their close connecting coupling, the classical error vanishes to 0. For (b), the situation is different. As visible in the network structure, only a classical coupling is present between main node 1 (connected to node 13) and node 2 (connected to node 16). The system behaves exactly as expected, because synchronisation is not possible due to the missing of a direct quantum link. In (c), this quantum link is present, however, both nodes are separated far from each other in the structure. As required, those nodes still synchronise, although some small deviations are visible in (c). Finally, in (d), when no connection is present, synchronisation simply cannot take place and the system runs out of sync.

These conclusions make the proposed system a valid suggestion for the future quantum network, as it possesses all required features. Further discussion will be enhanced in the next chapter.

4 Discussion

Most issues have already been mentioned before, but still require some attention due to the importance of their nature. These issues will be addressed in this chapter, and a discussion will be held about them.

4.1 Classical model

The classical ring network which was discussed in chapter 1 of the thesis exhibits an very unusual output. By tuning the network such that the network is a symmetrical ring, a configuration in which the movement goes to a synchronous state where all oscillators behave the same cannot be found. On the other hand, by choosing the amplification strength b_i different for each oscillator, a stable configuration can be found. This interesting principle was also observed by Nishikawa and Motter which they named *asymmetry-induced symmetry*. [11] An important conclusion here is that while trying to presume symmetry in your system, the output will not always exhibit the same symmetry as expected. This principle was used in the quantum network to define a more random structure to ensure stability.

The observation of a real correlation between the existence of a synchronous state for different oscillators and the non-existence for the same oscillators has not yet been found. A setup was made in Appendix 3, however, direct control on this matter is extremely difficult. Due to the rapid increase in size, analytic calculations are tedious. Perhaps some advances could be made in this process, e.g. finding out whether the synchronisation really depends on the complete parameter space, or if possibly some variables do not influence the actual stability of the system.

For the completely symmetrical network in which all oscillators are the same, the existence of the wave going around each node is extremely visible in a ring network structure. By adding an extra link in the 7-node ring network, this wave vanishes into thin air due to the vast changes in the structure. By expanding the network into more nodes, an interesting question arises: does the network also show the same phenomenon by introducing one extra (random) link in the large ring structure? Effectively, now two connected ring structures arise in which two waves can travel around. Further research shall we required to investigate the possibility of this happening.

4.2 Quantum model

After moving to the quantum model, the fidelity $\mathcal{F}$ was introduced. According to Li, Li and Song [9], this parameter is bounded above by 1, or at least does not exceed this value as it corresponds to complete synchronisation between the two optomechanical systems. In Figure 20 where the evolution for $\mathcal{F}$ is plotted, it is clear that the value exceeds 1 systematically. Although Li, Li and Song present this as a fact, I believe that due to quantum fluctuation the fidelity can temporarily rise above 1. My view is supported by Figure 3c) in their paper, in which lots of noise is present and the figure is cut off between 0 and 1. It is definitely not clear from their figure that the fidelity never exceeds 1. In future research, the discussed procedures and fidelity measures might be checked using the density operator, such that other synchronisation measures become available to verify the real quantum synchronisation of the system.

The major differences between the classical and quantum networks discussed in that the quantum model, sooner or later, introduces statistical effects that cannot be ignored. In the classical model, several expansions can be made using statistics, but it is no vital. External influences can be modelled in such a way, but it complicates the problem drastically, and it is therefore not advisable when it is not necessary. Apart from this, the setup is mathematically really comparable, since figures constructed from the equations of motion do not differ much in quantitative behaviour. Another for me rather unexpected agreement between the two domains is the nature of the synchronisation measure. In the classical model, the synchronisation can be measured using the Jacobi-matrix, which is significantly faster than examining or defining a method after constructing the complete integration process. In the quantum regime, the synchronisation methods S_c' and $\mathcal{F}$ are both based on the evolution of a covariance matrix of the perturbation operators. Both measures externally operate from the evolution. Or, to put it in other words, the question whether synchronisation is

possible can be answered before carrying out a simulation, thus saving much time trying to achieve such a process.

The proposed quantum model using coupled optomechanical systems is not yet available for practical applications. Aside from the technical (or experimental) challenges for the model, several consequences are not yet checked nor modelled. The first issue that might come to play is the time. The expected oscillations for the integration rapidly oscillate, and it requires a few thousands units ω_{m1} to achieve synchronisation. In the papers of Li, Li and Song and Mari et. al., this is not quite specified, as all parameters are considered in unit of other variables effectively making the variables dimensionless. A practical quantum internet needs to be fast, and not to cause any delay. The question whether the current network fulfils this requirement cannot be answered so future research is required (including experimental tests) to verify if this is possible.

Another possible issue is that the current system requires the initialisation setup to be empty of photons, that is $A_j = 0$. Some recent experiments show this is possible, however, this process should both be practical in real world circumstances and it should be fast enough as well. Another possibility is to investigate is whether this initialisation is really required for the system to operate. Further experimental research should and is being conducted to explore this matter.

Finally, nodes can be connected and disconnected at any time, solely due to the user's demand of the quantum internet. The suggested small world network is extremely useful for this, as it is set up to achieve this property right away. For other possibly researched network structures, the same principle should be checked carefully. This specific feature, which is vital for the network, makes me believe the small world network is just the right network for this communication process.

4.3 Future work

Since the model is constructed to be used as a quantum internet, multiple people should be using it at the same time. How and when could this issue be tackled using the model discussed? At least all users require to have several nodes at their possession at the same time or the network needs to be so fast that it handles all processes quickly after each other. Either of the two methods is a necessary constraint for the quantum network.

Just as the internet is being attacked every now and then by malicious people, the future quantum internet will be nothing different. For example, by removing a node altogether, is the network still able to synchronise? Or is synchronisation possible but only on a local scale? The network should function in a way that when a node is attacked, the whole network can still function as it normally would. This property could be examined by, for example, resilience patterns as discussed by Gao et. al. [5] By analysing the availability of resilience of the system, more information can be gathered to determine if this type of network is a useful type to perform as a quantum network.

Moreover, several expansions or tunings might be added to the system, including - but not limited to - the introduction of a directed electronic network by introducing new parameters K^+ and K^- to define the directionality of the network. This adds more flexibility in the precise construction of the network and adds the possibility to open or close yourself from the internet by either using an 'upload' or 'download' link from your node to the rest of the network. Apart from this, the connection strengths μ and K can be varied per node. Main nodes which only exist to send over information are more likely to require a strong connection to other large nodes. By further investigation, these decisions can be made more precise by calculation and trial.

5 Conclusion

In this bachelor thesis the availability of the quantum internet as a network of optomechanical systems was discussed. The classical ring network consisting of coupled oscillators following the Kuramoto model shows no synchronisation in a symmetric network and synchronises when the network is made asymmetrical. The final proposed quantum network in which separate quantum and classical couplings are used, assures us that the network fulfils the main requirements of the quantum network. The network is small world, indicating that a quick connection can be made. Furthermore, the network is separable so that multiple transactions can take place at the same time. Also, the network synchronises with quantum mechanically connected nodes, and not with others, as required.

Future recommendations include the further investigation in quantum measures and determining whether genuine quantum synchronisation takes place. This includes - but is not limited to - the fidelity $\mathcal{F}$ as well as the classical and quantum synchronisation measures for the proposed quantum network.

Moreover, it should be determined experimentally and theoretically whether the suggested optomechanical systems can be used in practice, i.e. are capable of working under real world circumstances and still assuring the same capabilities. After these challenges are either met or solved, the real quantum network will not lie too far away from us.

References

[1] Markus Aspelmeyer, Tobias J. Kippenberg, and Florian Marquardt. Cavity optomechanics. *Rev. Mod. Phys.*, 86:1391–1452, Dec 2014.

[2] Albert-László Barabási. *Network Science*. Cambridge University Press, first edition, Aug 2016. section 2.8, 3.8.

[3] Toon Beemsterboer. VS beschuldigen Rusland van hacken campagne, Oct 2016.

[4] Amber Dujardin, Wouter van Cleef, and Jan Kruidhof. Computersystemen plat na wereldwijde cyberaanvallen, May 2017.

[5] Jianxi Gao, Baruch Barzel, and Albert-László Barabási. Universal resilience patterns in complex networks. *Nature*, 530:307–312, Feb 2016.

[6] C. W. Gardiner and M. J. Collett. Input and output in damped quantum systems: Quantum stochastic differential equations and the master equation. *Phys. Rev. A*, 31:3761–3774, Jun 1985.

[7] David J. Griffiths. *Introduction to Quantum Mechanics*. Pearson, second edition. pg. 98 - 108.

[8] Aurelian Isar. Quantum fidelity of gaussian states in open systems. *Physics of Particles and Nuclei Letters*, 6(7):567, Nov 2009.

[9] Wenlin Li, Chong Li, and Heshan Song. Quantum synchronization and quantum state sharing in an irregular complex network. *Phys. Rev. E*, 95:022204, Feb 2017.

[10] A. Mari, A. Farace, N. Didier, V. Giovannetti, and R. Fazio. Measures of quantum synchronization in continuous variable systems. *Phys. Rev. Lett.*, 111:103605, Sep 2013.

[11] Takashi Nishikawa and Adilson E. Motter. Symmetric states requiring system asymmetry. *Phys. Rev. Lett.*, 117:114101, Sep 2016.

[12] Christian Pich. *Drawing Directed Graphs Clockwise*. Springer Berlin Heidelberg, Berlin, Heidelberg, 2010.

[13] Rik Sanders. Google opent tweede datacenter in Eemshaven, Dec 2016.

[14] Marlan O. Schully and M. Suhail Zubairy. *Quantum optics*. Cambridge University Press, first edition. pg. 271 - 275.

[15] C. Vuik, F. J Vermolen, M.B. van Gijzen, and M.J. Vuik. *Numerical Methods for Ordinary Differential Equations*. VSSD. pg. 83 - 84.

[16] Wikipedia. Kuramoto model, Nov 2016.

Appendix 1: The Laplacian matrix

The Laplacian matrix is a matrix which can be constructed directly from a given adjacency matrix **A**. Let's take an example with $n = 5$ nodes and $l = 12$ links in total. The graph is shown in Figure A1.1.

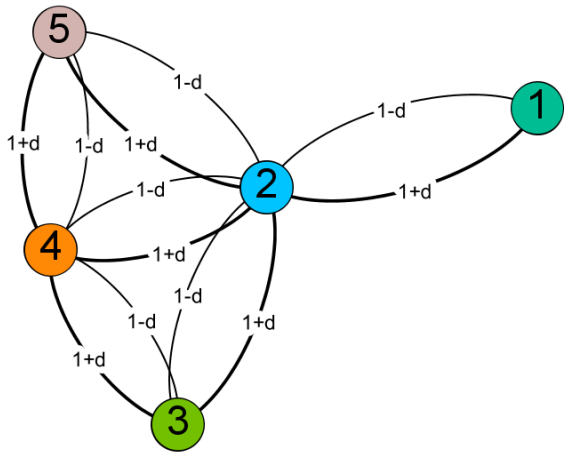

Figure A1.1: A network consisting of 5 nodes and 12 directed links. The Laplacian is considered for directed graphs as these are more general than undirected graphs. The weight of each link is also shown. Just as in the main text, the direction of the directed arcs is **clockwise**, thus node 1 receives input $1 + \delta$ and hands out $1 - \delta$ to node 2.

The corresponding adjacency matrix is shown below.

$$\mathbf{A} = \begin{pmatrix} 0 & 1+\delta & 0 & 0 & 0 \\ 1-\delta & 0 & 1+\delta & 1+\delta & 1+\delta \\ 0 & 1-\delta & 0 & 1+\delta & 0 \\ 0 & 1-\delta & 1-\delta & 0 & 1+\delta \\ 0 & 1-\delta & 0 & 1-\delta & 0 \end{pmatrix} \tag{A1.1}$$

Before the Laplacian matrix itself can be analysed, another concept is needed. The degree of a node k is the sum of the weights of all links the node has. When a matrix is directed, we define two cases: the incoming degree k^{in} and the outgoing degree k^{out}. Now the Laplacian matrix is defined as

$$\mathbf{L} = \mathbf{D} - \mathbf{A} \tag{A1.2}$$

where **D** is a diagonal matrix containing all outgoing degrees of all nodes and **A** is the adjacency matrix itself. For the example shown in Figure A1.1, the Laplacian will become

$$\mathbf{L} = \begin{pmatrix} 1+\delta & -1-\delta & 0 & 0 & 0 \\ -1+\delta & 4+2\delta & -1-\delta & -1-\delta & -1-\delta \\ 0 & -1+\delta & 2 & -1-\delta & 0 \\ 0 & -1+\delta & -1+\delta & 3-\delta & -1-\delta \\ 0 & -1+\delta & 0 & -1+\delta & 2-2\delta \end{pmatrix}. \tag{A1.3}$$

When the given matrix is not directional, the incoming and outgoing degrees are equal for every node. Both the adjacency matrix and the Laplacian matrix will be symmetric in this case. In general, this is not the case, as shown above.

Appendix 2: Analytic calculation of phase-synchronous states

The phase-synchronous states of a ring network with n nodes are tedious to calculate. In case there are two oscillators, the calculation can be done analytically.

First of all, fill in the given assumptions about the phase-synchronous state in the equations of motion as given by Eq. 2.5. That is, $\dot{r_i} = 0$ and $\dot{\theta_i} = \omega$ for all i. Then the following equations are found:

$$0 = r_i - 1 - \gamma r_i \sum_{j=1}^{n} \sin(\theta_j - \theta_i) \tag{A2.1}$$

$$0 = b_i(1 - r_i) + \varepsilon \sum_{j=1}^{n} A_{ij} \sin(\theta_j - \theta_i) \tag{A2.2}$$

Let's try to substitute Eq. A2.2 into the other one such that we only have the dependence of θ_i. Assume $r_i \neq 0$, because a trivial scenario in which an oscillator doesn't move at all isn't interesting. We get the following expression:

$$\frac{\varepsilon}{b_i} \sum_{j=1}^{n} A_{ij} \sin(\theta_j - \theta_i) - \gamma \left(1 + \frac{\varepsilon}{b_i} \sum_{j=1}^{n} A_{ij} \sin(\theta_j - \theta_i) \right) \sum_{j=1}^{n} \sin(\theta_j - \theta_i) = 0 \tag{A2.3}$$

Now we want to examine $n = 2$, which actually is the only case that can be solved analytically. To be fully correct, the case $n = 2$ does not even correspond to a ring network as two oscillators cannot define a ring at all but we will threat it to be a ring network anyway. The corresponding coupling matrix is given by

$$\mathbf{A} = \begin{pmatrix} 0 & 1+\delta \\ 1-\delta & 0 \end{pmatrix} \tag{A2.4}$$

This reduces Eq. A2.3 to a much simpler expression. Please note that the expression below is the formula corresponding to (θ_1).

$$\frac{\varepsilon}{b_1}(1+\delta)\sin(\theta_2 - \theta_1) - \gamma \left(1 + \frac{\varepsilon}{b_1}(1+\delta)\sin(\theta_2 - \theta_1) \right) \sin(\theta_2 - \theta_1) = 0 \tag{A2.5}$$

Since we are explicitly looking for phase-synchronous states, we may assume that $\theta_2 - \theta_1 \neq 0$. Apart from this, several combinations of $\theta_2 - \theta_1 = k\pi$ where $k \in \mathbb{Z}$ can occur. All these combinations are valid solutions as well. Now divide out $\sin(\theta_2 - \theta_1)$ to find out whether other situations are possible as well. After rearranging, we find

$$\sin(\theta_2 - \theta_1) = \frac{1}{\gamma} - \frac{b_1}{\varepsilon(1+\delta)} \tag{A2.6}$$

One may conclude directly that if $-1 \leq \frac{1}{\gamma} - \frac{b_1}{\varepsilon(1+\delta)} \leq 1$ there are more phase-synchronous solutions possible.

For $n \geq 3$ this method cannot be applied since all calculations greatly increase in difficulty. Particularly, one cannot obtain an equation like Eq. A2.5 since there is at least one extra dependence for other θ_i. This makes an analytic method impossible to find. We will therefore use numerical methods instead, also for the synchronous state.

Appendix 3: Results of optimal b in the classical ring network

This appendix contains the calculation of the optimal homogeneous b^* and inhomogeneous b_i as well as the corresponding Lyapunov exponent for the classical ring network. For the ring network, the parameters $\varepsilon = 2, \delta = 0.3$ are used as before.

Table 1: This table shows some examples of directed ring networks with size n. The value for γ is different for every n. Furthermore, when taking the best homogeneous value for b, stability does not occur (because $\Lambda^* > 0$) whereas for the inhomogeneous b_i, $\Lambda < 0$.

Nodes (n)	γ	b^*	Λ^*	b_i	Λ
3	0.65	2.6703	0.1735	4.3203 2.3537 2.8595	-0.0776
4	0.35	2.4040	0.1602	3.6276 2.6221 3.6335 1.4719	-0.1924
7	0.1	1.8685	0.1548	1.5252 0.3544 2.7715 4.1982 1.4578 0.6347 4.8224	-0.1563
10	0.04	1.6918	0.0986	7.3614 1.0674 0.2239 6.9967 1.8052 0.4849 1.8963 0.1639 0.8121 0.7052	-0.1448

For all mentioned networks, the same principle is observed. In a true symmetric network, synchronisation cannot take place due to a positive Lyapunov exponent whereas an asymmetric network does show synchronisation under special circumstances.

Notice that not all networks use the same values for γ. The reason for this is that the value for γ requires to be chosen in a specific way. We only need values for γ for which the homogeneous network is unstable and the inhomogeneous network is stable, not any other combinations of these. This is shown by the plot below for 3 nodes.

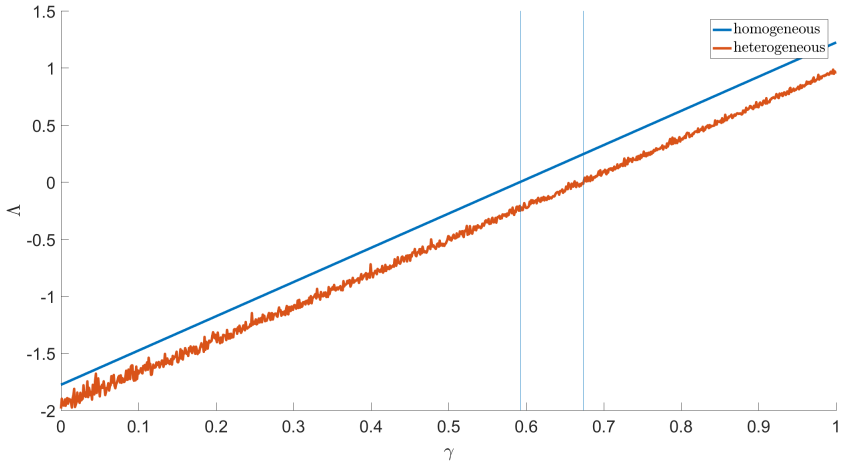

Figure A3.1: Plot of the value for γ versus the Lyapunov exponent for 3 nodes. The two vertical lines indicate the intersections for both lines for $\Lambda = 0$. In this domain, the theory explained is valid.

The plot was constructed using the procedure explained in Method 2, which explains the noise in the graph. Between $\gamma = 0.593$ and $\gamma = 0.674$, the theory discussed is applicable. This is indicated in Figure A3.1 by the vertical thin blue lines. When other values for γ are used, either both homogeneous and inhomogeneous variables result in a stable system or they both cause the system to destabilise. We see here that the possibility of such a system to occur at random is very rare, as only a small part of the spectrum shows the discussed behaviour.

Appendix 4: The dependence of ε on stability

By setting a reference value for ε_0, the Lyapunov exponent for other values of ε can be calculated easily. This principle was invented by Nishikawa and Motter. [11]

In order to visualize this, define λ as the eigenvalues of the Jacobian $\mathbf{J}$ with size $2n$. Furthermore, assume $\mathbf{I}$ to be the identity matrix with size $2n$. It follows from Eq. 2.8 that

$$\begin{aligned}\det(\mathbf{J}-\lambda\mathbf{I}) &= \det((-\gamma\mathbf{K}\ \mathbf{D}+\varepsilon\mathbf{L})+\lambda(\mathbf{D}-\gamma\mathbf{K})+\lambda^2\mathbf{I}) \\ &= \det\left(\frac{\varepsilon}{\varepsilon_0}\left(-\gamma\sqrt{\frac{\varepsilon_0}{\varepsilon}}\mathbf{K}\sqrt{\frac{\varepsilon_0}{\varepsilon}}\mathbf{D}+\varepsilon_0\mathbf{L}\right)+\frac{\varepsilon}{\varepsilon_0}\sqrt{\frac{\varepsilon_0}{\varepsilon}}\lambda\left(\sqrt{\frac{\varepsilon_0}{\varepsilon}}\mathbf{D}-\sqrt{\frac{\varepsilon_0}{\varepsilon}}\gamma\mathbf{K}\right)+\frac{\varepsilon}{\varepsilon_0}\left(\frac{\varepsilon}{\varepsilon_0}\lambda\right)^2\mathbf{I}\right) \\ &= \left(\frac{\varepsilon}{\varepsilon_0}\right)^n\det\left(\left(-\gamma\sqrt{\frac{\varepsilon_0}{\varepsilon}}\mathbf{K}\sqrt{\frac{\varepsilon_0}{\varepsilon}}\mathbf{D}+\varepsilon_0\mathbf{L}\right)+\sqrt{\frac{\varepsilon_0}{\varepsilon}}\lambda\left(\sqrt{\frac{\varepsilon_0}{\varepsilon}}\mathbf{D}-\sqrt{\frac{\varepsilon_0}{\varepsilon}}\gamma\mathbf{K}\right)+\left(\frac{\varepsilon}{\varepsilon_0}\lambda\right)^2\mathbf{I}\right)\end{aligned} \tag{A4.1}$$

Now introduce $\gamma' = \gamma\sqrt{\frac{\varepsilon_0}{\varepsilon}}, \lambda' = \lambda\sqrt{\frac{\varepsilon_0}{\varepsilon}}$ and $\mathbf{D}' = \mathbf{D}\sqrt{\frac{\varepsilon_0}{\varepsilon}}$. Note that these variables can be calculated if both ε and ε_0 are known. Then we have

$$\det(\mathbf{J}-\lambda\mathbf{I}) = \left(\frac{\varepsilon}{\varepsilon_0}\right)^n\det\left(\left(-\gamma'\mathbf{K}\mathbf{D}'+\varepsilon_0\mathbf{L}\right)+\lambda'\left(\mathbf{D}'-\gamma'\mathbf{K}\right)+\left(\lambda'\right)^2\mathbf{I}\right) \tag{A4.2}$$

For a known stability for ε_0, the stability for an arbitrarily ε can be calculated by using Eq. A4.2. Therefore we set $\varepsilon = 2$ as a reference value throughout the report.

Appendix 5: The S matrix

The system of equations for the perturbation is already linearised, so the only goal we have is to write them in a matrix method. This is done in Eq. 3.32, such that we find

$$\mathbf{S} = \begin{pmatrix} -\kappa & -\Gamma_1 & 0 & 0 & -2gIm[A_1] & 0 & 0 & 0 \\ \Gamma_1 & -\kappa & 0 & 0 & 2gRe[A_1] & 0 & 0 & 0 \\ 0 & 0 & -\kappa & -\Gamma_2 & 0 & 0 & -2gIm[A_2] & 0 \\ 0 & 0 & \Gamma_2 & -\kappa & 0 & 0 & 2gRe[A_2] & 0 \\ 0 & 0 & 0 & 0 & -\gamma & \omega_{m1} & 0 & -\mu \\ 2gRe[A_1] & 2gIm[A_1] & 0 & 0 & -\omega_{m1}(1+C_1(t)) & -\gamma & \mu & 0 \\ 0 & 0 & 0 & 0 & 0 & -\mu & -\gamma & \omega_{m2} \\ 0 & 0 & 2gRe[A_2] & 2gIm[A_2] & \mu & 0 & -\omega_{m2}(1+C_2(t)) & -\gamma \end{pmatrix} \tag{A5.1}$$

Appendix 6: The small world network

A random network is called a small world network if every node can reach any other node by passing only a few other nodes. This measure is vague, but recent attention by Barabási introduced some more quantitative measures. [2] The first important measure of a network is the so called network diameter d_{max}. This is defined as the longest distance from any node to any other node. Furthermore we may also define the average path length $\langle d \rangle$, which is the average distance between all pairs of nodes in the network. Furthermore, as introduced in Appendix 1, we recall the degree k of node which is the number of links it has. Now we may define the average degree $\langle k \rangle$ as the average number of links a node has in the network.

Now we are able to define a quantified measure of 'being a small world network' as

$$\langle d \rangle = \frac{\ln N}{\ln \langle k \rangle} \tag{A6.1}$$

where N is the total number of nodes. If this equation is satisfied, then the network can be called a small world network. [2]

For the small networks discussed in the main text, this insight cannot be used. Since the network is always small, the shortest distance will always be short. Therefore we look into the situation where we have 200 main nodes and 874 sub nodes. This is a total of $N = 1074$ nodes. This is also more realistic when regarding the real future quantum internet. The following figure was constructed.

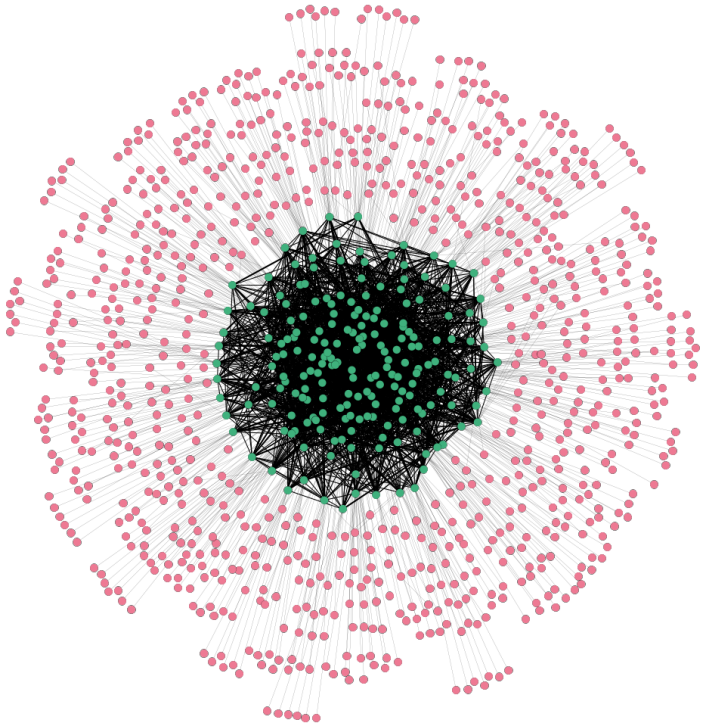

Figure A6.1: Schematic representation of the small world network with 200 main nodes and 874 sub nodes. The green nodes coupled by the thick black lines are the main nodes and the outer nodes connected by thin lines are the sub nodes. Random quantum links between main nodes are present as well, indicated by the spider web of black lines in the middle of the figure.

Simulations and calculations show that for this network, $\langle k \rangle \approx 5.648$. Using Eq. A6.1, we find $\langle d \rangle = 4.03$. Since $\langle d \rangle \approx 3.598$, this network can be called a small world network.

Appendix 7: Matlab scripts

All numerical integrations and adjacency matrices were constructed using Matlab. All scripts are over 100 lines long because they were constructed to be easily adaptable. Therefore, all scripts can be downloaded as a zip file using the following link: `http://g2f.nl/0m1nhvm`